Experimental study of filling and emptying of a large-scale pipeline

EINDHOVEN UNIVERSITY OF TECHNOLOGY
Department of Mathematics and Computer Science

CASA-Report 12-15
May 2012

Experimental study of filling and emptying of a large-scale pipeline

by

Q. Hou, A.S. Tijsseling, J. Laanearu, I. Annus, T. Koppel, A. Bergant, S. Vučkovič, J. Gale, A. Anderson, J.M.C. van 't Westende, Z. Pandula, A. Ruprecht

Centre for Analysis, Scientific computing and Applications
Department of Mathematics and Computer Science
Eindhoven University of Technology
P.O. Box 513
5600 MB Eindhoven, The Netherlands
ISSN: 0926-4507

Experimental study of filling and emptying of a large-scale pipeline

Q. Hou[1], A.S. Tijsseling[1], J. Laanearu[2], I. Annus[2], T. Koppel[2],
A. Bergant[3], S. Vučkovič[3], J. Gale[3], A. Anderson[4], J.M.C. van 't Westende[5], Z. Pandula[6], A. Ruprecht[7]

[1]*Eindhoven University of Technology, The Netherlands*
[2]*Tallinn University of Technology, Estonia*
[3]*Litostroj Power d.o.o., Ljubljana, Slovenia*
[4]*Newcastle University, United Kingdom*
[5]*Deltares, Delft, The Netherlands*
[6]*Budapest University of Technology, Hungary*
[7]*University of Stuttgart, Germany*

Abstract

The filling with liquid of an initially empty pipeline and its counterpart, the draining of an initially liquid-filled pipeline, are of great interest due to the many practical applications. Several potential problems may occur, of which water-hammer and slug impact are the most important. To investigate the filling and emptying processes, different mathematical models have been proposed, in which a common assumption is that the water column evolves with unchanged front and/or tail. This is a reasonable assumption for small-scale systems, particularly in cases with relatively high upstream pressure head and low downstream resistance. However, it is not clear whether this assumption is applicable to large-scale systems. This issue is of high importance for the development of air pockets and gravity currents in pipelines during filling and draining processes.

This study presents the experimental results of the flow behaviour during the rapid filling and emptying of a large-scale pipeline. The experimental apparatus was designed and built at Deltares, Delft, The Netherlands, as part of the EC Hydralab III project. Different from other laboratory studies, the scale of this experiment is close to the practical situation in many industrial plants. The test rig includes a variety of components (e.g. tanks, flow meters, valves, pipes of different materials) and the operation procedure is rather complex. The flow behaviour is measured by various instruments and hence a thorough hydrodynamic analysis is possible. All these features make the current study particularly useful as a test case for real filling and draining situations.

In the filling of an initially empty pipeline, the focus was on the overall behaviour of the lengthening water column and the water-air interface evolution. In the emptying of an initially water-filled pipeline, together with the hydrodynamics of the shortening water column, the shape and behaviour of the water tail (air-water interface) was investigated. Thirteen different combinations of initial upstream driving air pressure and downstream valve resistance were tested. The influence of these two factors on the outflow rate is clarified. It was confirmed that both the inflow front in filling and the outflow tail in emptying do not entirely fill the pipe cross section. Shape changes occur at both the water-air and air-water interfaces. Although the flow regime transition is a rather complex phenomenon, certain features of the transition pattern are observed and explained qualitatively and quantitatively.

Keywords: Pipe filling and emptying, two-phase flow, large-scale pipelines, air-water and water-air interface evolution, flow-regime transition

1. Introduction

Rapid pipe filling and emptying occur in various hydraulic applications, such as water-distribution networks, storm-water and sewage systems, fire-fighting systems, oil transport pipelines and pipeline cleaning. With respect to rapid filling of an empty pipeline, while the water column is driven by a high head, air is expelled by the advancing water column. If the generated air flow is not blocked by valves, the water column grows with little adverse pressure and attains a high velocity. For emptying of a pipeline initially filled with water, while the air is blown into the pipeline, water is expelled out of the system. If the driving air pressure is high and the resistance from pipe components is low,

the water column shortens with high acceleration and a high velocity as a result. When the advancing column in pipe filling and draining processes is suddenly stopped (fully or partially), severe pressure changes occur in the system (see e.g. Guo & Song 1990 [8], Zhou *et al.* 2002 [28], Martino 2008 [17]).

Rapid filling processes in hydraulics have been experimentally and theoretically studied. The laboratory tests performed by, among others, Nydal & Andreussi (1991) [18], Liou & Hunt (1996) [13], Zhou *et al.* (2002) [27, 28] and Vasconcelos *et al.* (2004) [22, 23, 24] were based on relatively short pipes of small diameters. The pipe emptying problem did not receive much attention in literature. One investigated problem is bubble motion in liquids in horizontal, vertical and inclined tubes due to gravity (see e.g. Zukoski 1966 [29], Benjamin 1968 [2]). The theoretical and experimental studies on this problem were summarized by Shosho & Ryan (2001) [20]. The focus of Zukoski (1966) [29] was on the effect of viscosity, surface tension, inclination angle and pipe diameter on the bubble's movement. It was found that for Reynolds numbers greater than about 200, the bubble propagation rates are substantially independent of viscous effects. Surface tension is negligible when its value is less than 10 percent of $\Delta\rho g r^2$, where r is the tube radius, g is the gravitational acceleration and $\Delta\rho$ is the absolute value of the density difference between the primary and bubble fluid. Steady inviscid gravity currents in horizontal tubes were theoretically examined by Benjamin [2]. It was found that the flow celerity of both the bubble and the gravity current is $0.5\sqrt{gD}$, where D is the tube diameter. For rapid pipe filling and emptying in hydraulics [13, 18, 22, 27, 28], both Reynolds number and pipe diameter are generally large. Consequently, the effect of viscosity and surface tension on the bubble motion is negligible.

For filling a small-scale system with relatively high driving head, the deformation of the water front shape has an insignificant effect on the overall hydrodynamics of the lengthening water column [9]. Thus a vertical water-air interface is often assumed to characterize the advancing flow. However, it is not clear in advance whether this assumption of a plane water front will be applicable to large-scale pipelines. The new large-scale tests aim at a better understanding of the flow hydrodynamics in the filling and emptying processes. We focus on the evolution of the moving interface and its effect on the pressure distribution and inflow and outflow rates. To determine the dynamic characteristics of the viscoelastic PVC pipeline, water-hammer tests were performed and numerically validated. These are out of the range of the report and are presented elsewhere [5, 10].

The rest of the report is as follows. Section 2 gives detailed information on the experimental apparatus including its components, measuring instruments and data acquisition equipments. In Section 3 the experimental procedures for filling and emptying are presented and variable-settings in the emptying tests are described. The experimental results are presented in Section 4 with focus on the flow rate, the evolution of the water front (filling) and tail (emptying) and the pressure variation. The rigid-column simulation of filling is presented in Section 5. Conclusions are summarized in Section 6.

2. Experimental apparatus

The piping system used in the experiments is illustrated in Fig. 1. This Deltares two-phase facility was rebuilt from the previous experiment performed by Lubbers [14]. The main difference is cutting the pipeline to 300 m from 600 m. The experimental apparatus consisted of a water tank, an air tank, steel supply pipelines (for water and air), a PVC inlet pipe, a pipe bridge, a horizontal long PVC pipeline (the test section), an outlet steel pipeline and a basement reservoir. The detailed information is given below, and part of it can be found in [11, 12].

2.1. System origin and coordinates

The downstream end of the PVC pipe bridge was defined as the origin of the coordinate system. It is the starting point of the test section. The x-coordinate follows the central axis of the pipeline, the y-coordinate is not used herein and the z-coordinate is the vertical elevation. Coordinates of measuring instruments and other important components are shown in Fig. 2.

2.2. Tanks and pipes

A water tank (see Fig. 3) with a constant 25 m head relative to the centre line of the inlet (see Fig. 4a) was used to supply water in the filling experiment and an air tank with a 70 m^3 volume was used to supply air in the emptying experiment. The water supply steel pipe, from the T-junction ($x = -27.2$ m, in practice it is a short Y-junction (see

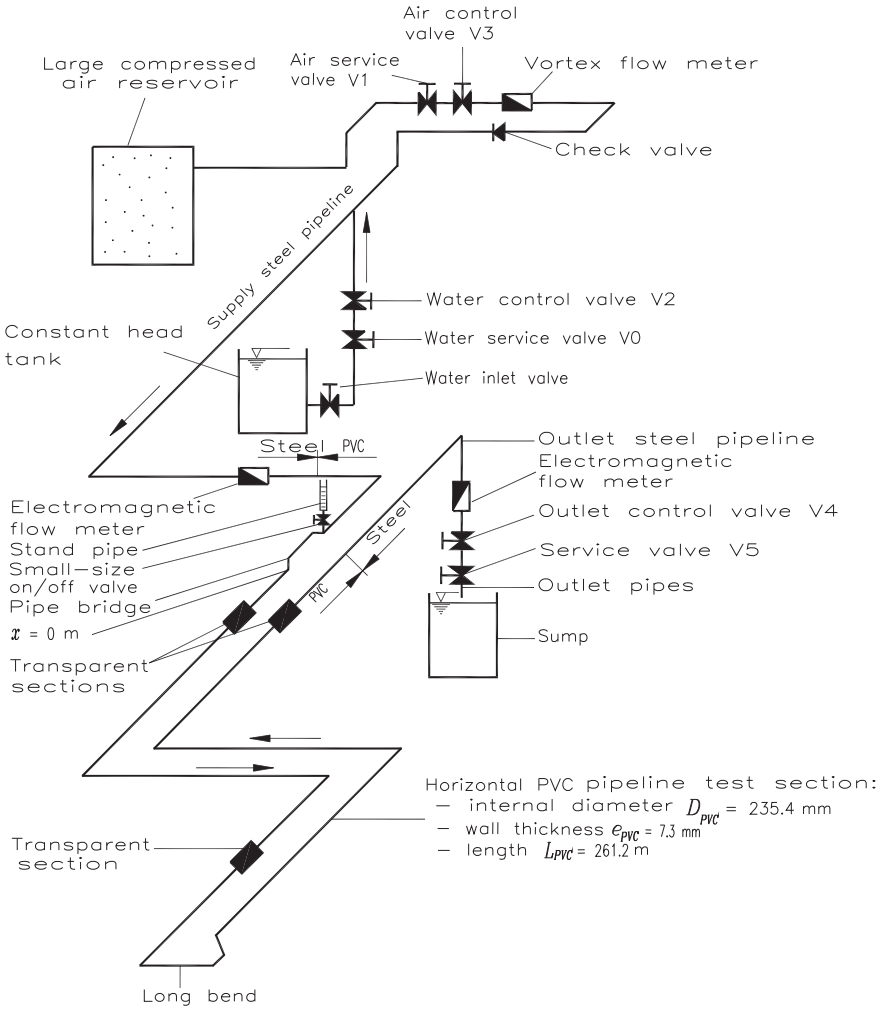

Figure 1: Sketch of the large-scale PVC pipeline apparatus at Deltares, Delft, The Netherlands. Adapted from [5].

Fig. 5), but it is not important in view of the large-scale) to the upstream steel-PVC connection ($x = -14$ m), was 13.2 m long. The air supply steel pipe, from the check valve ($x = -43.1$ m) to the T-junction, was 15.9 m long. The vertical leg of the T-junction was 3.6 m long. The inner diameter of the steel pipes was 206 mm, with a wall thickness of 5.9 mm. The PVC pipe was 275.2 m long and its diameter was 250 mm with an average wall thickness of 7.3 mm. It consisted of two parts. The first part included a PVC inlet pipe and a pipe bridge. It was from the upstream steel-PVC connection to the selected starting point of the test section ($x = 0$ m) and its length was 14 m. With the aid of a piezometer tube, the bridge was used to set up the initial water column for pipe filling. The second part was the horizontal PVC pipe of length 261.2 m (from $x = 0$ m to the downstream PVC-steel connection). Most of the measurements took place in this section. The outlet steel pipe connected the downstream end of the PVC pipe to the basement reservoir. It contained two "segments" of different diameter connected by a reducer. The reducer had a length of 0.3 m and located 0.3 m upstream of the outlet flow meter. The first segment was 8.8 m long and the diameter was 250 mm with a wall thickness of 7 mm. The second segment was 2 m long and the diameter was 200 mm with a wall thickness of 5 mm.

The upstream inlet and downstream outlet steel pipe segments are shown in Fig. 4, and the corresponding CAD drawing is depicted in Fig. 5.

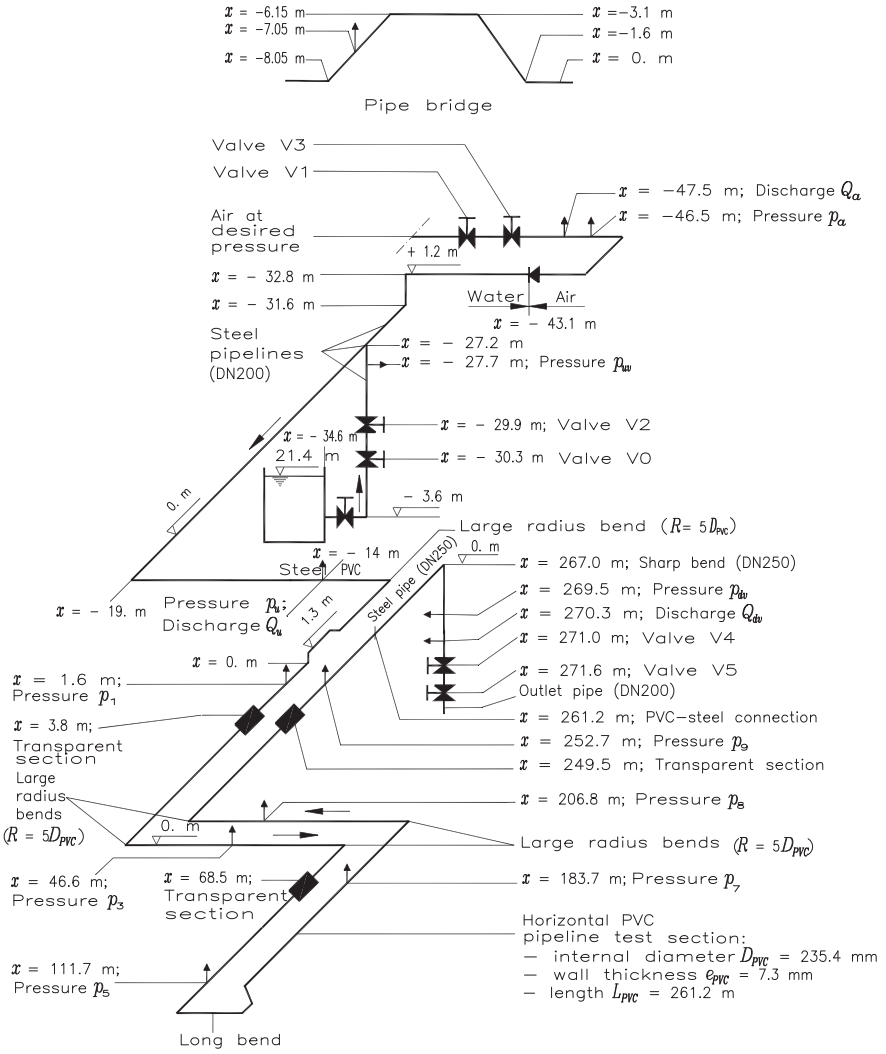

Figure 2: System dimensions and coordinates of the measuring instruments. Adapted from [5].

2.3. Supports and connections

To suppress pipe motion and associated FSI effects [4, 5, 10, 21, 25], it was attempted to structurally restrain the pipe system as much as possible. The PVC pipeline was fixed to the concrete floor by metal anchors and supported with wooden blocks to reduce sagging (see Fig. 6a). The pipe bridge – elevated 1.3 m above the main pipeline axis – was supported by a tube-frame (see Fig. 6a). However, it appeared hard to fix the most downstream elbow; at this point a very heavy mass was attached with a rope so to reduce its vertical movement (see Figs. 4b and 5). The PVC pipeline segments were attached to each other by bolted connections and flanges (see Fig. 6a). Wherever the PVC pipe needed to turn its direction, a large radius bend ($R = 5D_{PVC}$) was used. There were four 90-degree bends in the test section as shown in Fig. 2. A long bend was used at the 180 degree turning point as exhibited in Figs. 2 and 6b.

2.4. Valves

There were nine valves in the system as shown in Fig. 1. Several small air venting valves are not shown; these mainly located upstream of the pipe bridge. The check valve ($x = -43.1$ m) was used to prevent entrance of water into the air system. The water inlet valve ($x = -34.6$ m, unlabelled) connected to the water tank remained open during all experiments. The remaining seven valves numbered from V0 to V6 were actively operated manually or automatically

Figure 3: The water tank with a constant 25 m head at Deltares, Delft, The Netherlands. It has been brought down in 2011.

(*a*) (*b*)

Figure 4: Laboratory view: (a) upstream and (b) downstream steel pipes.

in the experiments (see Figs. 1, 2 and 5). Three of them (valves V0, V2 and V6) were used in the filling process. The upstream service valve V0 (DN200) was operated manually to supply water. The automatic control valve V2 (DN150) was used for flow regulation. A small-size on/off valve V6 in a transparent stand pipe located at the upstream end of the pipe bridge (see Figs. 1 and 7a) was used for monitoring the initial front of the water column. Four valves (V1,V3,V4 and V5) were used in the emptying process. The manually operated valve V1 (DN300) was used to supply air into the system. The automatically operated valve V3 (DN250) at five diameters distance from V1 was used to regulate the air flow. The downstream manual valve V4 (DN200) was used to regulate the outflow. Its orifice was maximally open at 0 degree position and fully closed at 90 degree position (with ruler as shown in Fig. 7b). The relative positions from 9/9-opening to 0/9-opening are henceforth used to characterize the outflow conditions. The manually operated on/off valve V5 (DN200), mounted three diameters downstream from V4, was used to start the

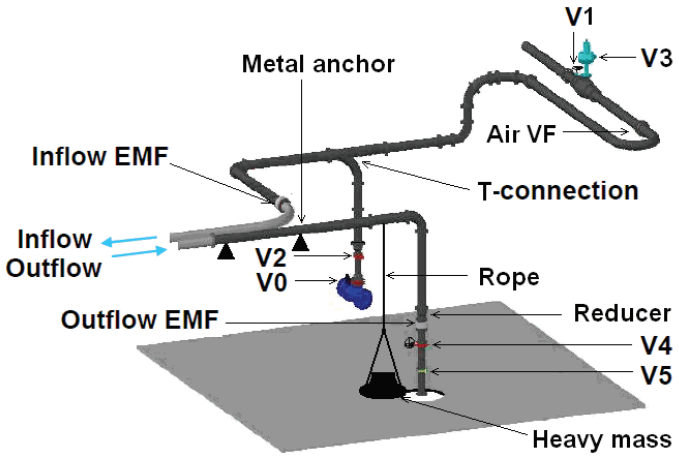

Figure 5: Upstream and downstream steel pipe segments and valves: CAD drawing.

emptying process. All valves were butterfly valves except valve V3, which was a cage valve.

2.5. Instruments and data acquisition

2.5.1. Measuring instruments

A maximum of 28 instruments were installed along the whole system as sketched in Fig. 8. There were twelve pressure transducers, six water level meters, four thermometers, three void fraction meters and three flow meters. The coordinates of the pressure transducers and flow meters are shown in Fig. 2. The coordinates of the other measuring instruments are listed in Table 1, where the type, output range, position (within pipe cross-section) and other detailed information is provided. The three transparent sections had lengths of 0.7 metres with transparent windows 0.5 metres long. A high-speed camera set up at these sections (see Fig. 8) recorded the water-air (filling) and air-water (emptying) interface shapes and the air-water mixing process. A removable accelerometer was used to measure pipe vibration amplitude and frequency caused by impacting liquid slugs. The measuring sections were numbered in sequence from upstream to downstream and the instruments were accordingly labelled as indicated in Table 1.

It was found that the pressure transducer p_{dv} at $x = 269.5$ m and the vertex flow meter at $x = -47.5$ m did not work properly. Hence their measurements are not used in the following data analysis.

2.5.2. Uncertainties

According to nominal values provided by the manufactures, the estimated uncertainty for steady-state conditions was ± 1.0% in the flow-rate measurements, ± 0.1% in the pressure measurements, ± 0.8 °C in the temperature measurements and ± 15 mm in the water-level measurements. All pressure transducers were of the strain-gauge type with a natural frequency of 10 kHz. They were all installed flush-mounted as good as possible.

Apart from the uncertainties in the measurements, there were few uncertainties in the filling and emptying process itself. First, the response time of the measuring instruments is different. For example, the difference between the response time of p_u ($x = -14$ m) and upstream electromagnetic flow meter (EMF, $x = -14.3$ m) was about 1 second. The response time of upstream EMF was taken as $t = 0$ in pipe filling, and the response time of downstream EMF was taken as $t = 0$ in pipe emptying. Second, the PVC pipeline was assumed initially empty in each pipe filling run. However, it was found that some water remained between the sections 3 and 8 after a filling and subsequent emptying run. The amount of uncleared water varied per test. When valve V4 was fully open and high pressure air (more than 1 bar) was used to empty the pipe, the level of remaining water was about 30 mm on average. The water level was up to 60 mm when low pressure air (less than 1 bar) was used for draining. The remaining water is mainly attributed to pipe skin friction and turbulence. Third, before a pipe filling run, the air entrapped in the steel pipe between the T-connection and the check valve was not released. It is not clear what is its effect on the filling process.

Table 1: DAQ channel setting and instruments with coordinates and section labelling.

DAQ channel	output	mark	coordinate (m)	section	range	position	type	data column
–	time	–	–	–	0 – 200000 s	–	–	1
0	pressure	p_{air}	-46.5	air inlet	0 – 10 bar	top	strain-gauge	2
1	temperature	T_{air}	-46.3	air inlet	-100 – 300 °C	top	platinum resistance	3
2	flow rate	Q_{air}	-47.5	air inlet	0 – 500 L/s	–	vertex	4
3	pressure	p_t	–	air tank	0 – 10 bar	–	strain-gauge	5
4	flow rate	Q_u	-14.3	inlet steel pipe	0 – 500 L/s	–	electromagnetic	6
5	pressure	p_u	-14.0	inlet steel pipe	0 – 5 bar	left-side	strain-gauge	7
6	flow rate	Q_{dv}	270.3	outlet steel pipe	0 – 500 L/s	–	electromagnetic	8
7	pressure	p_1	1.6	1	0 – 5 bar	right-side	strain-gauge	9
8	pressure	p_{3t}	46.6	3	0 – 5 bar	top	strain-gauge	10
9	pressure	p_{3b}	46.6	3	0 – 5 bar	bottom	strain-gauge	11
10	pressure	p_5	111.7	5	0 – 5 bar	right-side	strain-gauge	12
11	pressure	p_7	183.7	7	0 – 5 bar	right-side	strain-gauge	13
12	pressure	p_8	206.8	8	0 – 5 bar	right-side	strain-gauge	14
13	pressure	p_9	252.8	9	0 – 5 bar	right-side	strain-gauge	15
14	water-level	WL_1	1.7	1	12.163 mm/V	top-bottom	conductivity	16
15	water-level	WL_3	46.4	3	12.135 mm/V	top-bottom	conductivity	17
16	water-level	WL_5	111.7	5	12.318 mm/V	top-bottom	conductivity	18
17	water-level	WL_7	183.7	7	11.932 mm/V	top-bottom	conductivity	19
18	water-level	WL_8	206.8	8	12.246 mm/V	top-bottom	conductivity	20
19	water-level	WL_9	252.9	9	12.178 mm/V	top-bottom	conductivity	21
20	temperature	T_1	1.6	1	0 – 50 °C	left-side	platinum resistance	22
21	temperature	T_2	46.4	3	0 – 50 °C	right-side	platinum resistance	23
22	temperature	T_3	252.8	9	0 – 50 °C	left-side	platinum resistance	24
23	void fraction	VF_1	0.5	1	0 – 100 %	left-side	conductivity	25
24	void fraction	VF_6	141.9	6	0 – 100 %	right-side	conductivity	26
25	void fraction	VF_9	251.7	9	0 – 100 %	left-side	conductivity	27
28	pressure	p_{dv}	269.5	outlet steel pipe	0 – 5 bar	right-side	strain-gauge	28
29	pressure	p_{uv}	-27.7	inlet steel pipe	0 – 5 bar	right-side	strain-gauge	29

(a)

(b)

Figure 6: Laboratory view: (a) PVC pipe bridge with the supporting tube-frame and pipe anchors and (b) long turn.

2.5.3. Data acquisition

Deltares' 32-channel data acquisition system DAQ was used for synchronized recording of flow rate (inflow Q_u, outflow Q_{dv}, air flow Q_a), pressure (p_1, p_{3t}, p_{3b}, p_5, p_7, p_8, p_9), temperature (T1, T3, T9), water level (WL1, WL3, WL5, WL7, WL9) and void fraction (VF1, VF3, VF9); see Fig. 8. Video camera and accelerometer recordings were not electronically synchronized with the data acquisition system DAQ recordings. The used channels of the DAQ system are listed in Table 1. A sampling rate of 100 Hz was used to record the experimental quantities: discharge, gauge pressure, water level, void fraction and temperature.

3. Experimental variables and procedure

3.1. Experimental variables

All pipe filling experiments were carried out with the downstream valves V4 and V5 fully open and a constant driving head of 21.4 m ($x = -34.6$ m, relative to $z = 0$ m). In the pipe emptying tests, two different experimental variables were systematically investigated. The first one was the upstream driving air pressure, chosen because it highly affects the air-water interface movement. Five different air pressures were used in this investigation. They were 2, 1.5, 1, 0.5 and 0 barg. The last case implies that the draining is due to gravity only (driven by the downstream

(a) (b)

Figure 7: Laboratory view: (a) small on/off valve (piezometer) at pipe bridge and (b) manually operated outflow control valve (V4) with ruler.

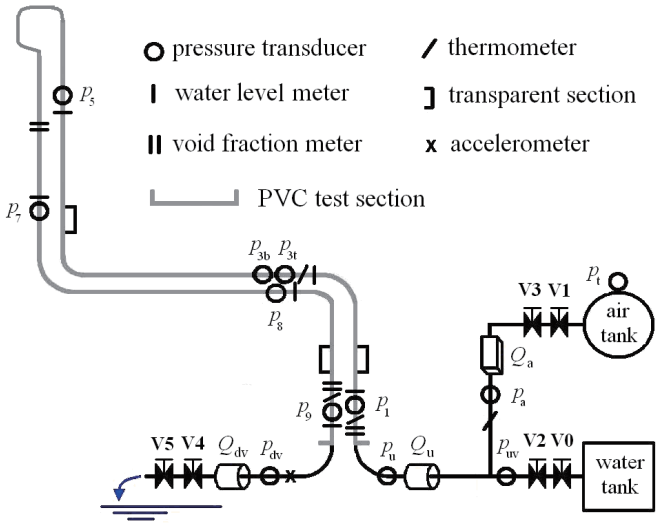

Figure 8: Layout of measuring instruments in the large-scale PVC pipeline apparatus.

vertical pipe segment, i.e. siphon). The second experimental variable was the degree of opening of the outlet control valve V4 (0 degrees – fully open; 90 degree – fully closed). By changing the opening position of valve V4 different outflow rates are obtained and the corresponding movement of the air-water interface is largely affected. Five different valve openings were tested. They were 9/9, 8/9, 6/9, 4/9 and 2/9 open, and were characterized as 0/9, 1/9, 3/9, 5/9 and 7/9 closing of valve V4 in [12]. Not all the test options were combined and the thirteen test conditions used are listed in Table 2.

3.2. Experimental procedure

To describe the procedure for pipe filling and emptying experiments, Fig. 5 is used.

3.2.1. Filling

In the pipe filling experiments, air at atmospheric pressure initially present in the system is replaced by water. Both downstream valves V4 and V5 are initially open. First, the upstream valve V0 was opened manually. Then the

Table 2: Variables settings in the emptying experiments (valve V4 setting: 9/9 fully open, 0/9 fully closed).

Case	1	2	3	4	5	6	7	8	9	10	11	12	13
$p_a^{\dagger}$	2.0	1.5	1.0	0.5	0.0	2.0	2.0	2.0	2.0	1.0	1.0	1.0	1.0
$\phi^{\ddagger}$	9/9	9/9	9/9	9/9	9/9	8/9	6/9	4/9	2/9	8/9	6/9	4/9	2/9

† tank air pressure (barg); ‡ dimensionless valve opening.

automatic valve V2 was opened from 0% to 15% until the height of the water in the pipe bridge reached a level of 0.4 metre (0.04 barg reading from pressure transducer p_u at $x = -14$ m as shown in Fig. 2). After closing valve V2 the water level gradually approached the desired height (1 m) due to a small leakage of V2. When the required water level of 1 m was reached ($x = -6.5$ m), as visually observed from the small transparent stand pipe (see Fig. 7a), the small-size on/off valve on it was closed, and valve V2 was fully opened immediately. Then the filling process started at $t = 0$. After some time (about three minutes) a steady state was reached, i.e. the inlet and outlet flow discharges were equal and constant. Then the outlet control valve V4 was closed slowly from 0 to 75 degrees to avoid possible pressure surges. After the gradual closure of valves V5 and V2 the filling process was completed.

3.2.2. Emptying

Water entirely filling the pipeline was driven out by compressed air from the upstream high-pressure tank (pressure initially fixed between 0 barg and 2 barg). The initial conditions for each emptying run were established by the completed filling process. Air entrapped in the high-elevation air supply line (elevation 1.2 m) was ventilated through the small-size air-venting valve mounted five diameters downstream of the check valve. Similarly, air entrapped in the pipe bridge was released by a ventilating hose connected to its top. Water supply valve V0 was then manually closed, so that the unwanted leakage of valve V2 in closed position was eliminated. Then valve V4 was set to the desired degree of closing for a controlled emptying process. After valve V1 was opened (valve V3 was always open at 15% for flow regulation), the static water-column in the system was pressurized by the high-pressure air. When the induced pressure oscillations had become small enough, the downstream valve V5 was opened manually as quickly as possible and then the emptying process started at $t = 0$. After the main air-water interface arrived at the pipe end and all water slugs were driven out of the system, valve V1 was closed and the emptying process was considered completed.

In fact, the filling and emptying experiments were continuously performed one after the other. The whole procedure including initialization for filling, pipe filling, steady-state water flow, initialization for emptying (air ventilation, valve V4 adjustment and water-column pressurization) and pipe emptying is detailed in Table 3. For every test, the runs were repeated at least five times for nominally the same initial and boundary conditions to assess the repeatability of the unsteady two-phase flow in the pipeline and to enable statistical and error analysis.

4. Experimental results

4.1. Steady-state water flow

Seventy eight steady-state flow measurements have been carried out in between the filling and emptying experiments, and eight of them were used to determine the head losses due to skin friction and due to the long 180 degree bend (see Fig. 2). The Darcy-Weisbach formula was used to find the friction factor f and minor-loss coefficient K_{lb} at the long bend. The 90 degree bends are assumed to be without loss because of their large radius of curvature ($R = 5D_{PVC}$). The time-averaged flow rates measured by upstream and downstream EMFs, together with averaged pressure-heads recorded by p_1 and p_5, were used to calculate the f values. The coefficient K_{lb} was calculated using the measured head loss of the pipeline segment between sections 5 and 7 (see Fig. 8). The results of eight steady-state flow experimental runs (see Table 4) confirm that the head loss due to the 180 degree turn is negligible.

The measured flow rates, together with time-averaged pressure-heads from p_1 and p_9, were then used to calculate the friction factors, which all eight were nearly the same as shown in Table 4. The velocity of the steady flow is about 4 m/s. The Reynolds number is about 950000. Knowing the Reynolds number Re and the corresponding friction factor,

Table 3: Experimental procedure for a complete pipe filling and emptying cycle.

Step	Operation	Description	Note
1	Start recordings	Air tank pressurization to desired value before or during filling	
2	Open manually V0	Open downstream valves V4 and V5	Initialization for filling
3	Open automatically V2 from 0% to 15 %	Wait until pressure p_u rises up to 0.04 bar (vertical pipe filling)	
4	Open automatically V2 from 15% to 0 %	Wait until pressure p_u rises up to 0.1 bar (water level in pipe bridge)	
5	Open automatically V2 from 0% to 100 %	Fill until system is steady and wait for 60 seconds	Filling starts
6	Close manually V4 from 0 degree to 75 degrees (gradually)	Also V2 closing started	
7	Close automatically V2 (gradually)	Also close manually V5 (gradually)	Filling ends
8	Ventilate system including air supply pipe downstream of check valve and pipe bridge		Initialization for emptying
9	Close manually V0	System pressure less than air pressure	
10	Set manually V4 to desired degree		
11	Open manually V1 and V3 is always opened to 15%	Pressurize system and wait for 60 seconds for stabilization	
12	Open manually V5 as quickly as possible	Air pressure drops during emptying	Emptying starts
13	Close manually V1	Before closing V1 wait until all slugs are out (visual and audible inspection)	Emptying ends
14	Stop recordings		

Table 4: Results of steady state tests.

Run	Re	f	ε/D_{PVC}	K_{lb}
1	947670	0.0137	0.0001108	0.0584
2	947890	0.0137	0.0001112	0.0553
3	948710	0.0136	0.0001096	0.0533
4	947690	0.0136	0.0001086	0.0501
5	948040	0.0136	0.0001092	0.0608
6	948950	0.0136	0.0001074	0.0629
7	947720	0.0136	0.0001097	0.0691
8	950680	0.0136	0.0001044	0.0610

the pipe relative roughness, i.e. the ratio of equivalent roughness size to pipe diameter ε/D_{PVC}, can be calculated from the Colebrook-White formula. The calculated relative roughness is about 0.00011, which is slightly smaller than that of the DN50 PVC pipe (0.00015) used in [13].

The hydraulic grade line for the PVC pipe is straight as shown in Fig. 9. This is consistent with the above calculated negligible head loss due to the 180 degree long turn. The measured pressure head at $x = -27.7$ m is 13.5 m. The large head loss $21.4 - 3.1 - 13.5 = 4.8$ m at the very beginning is because of the head losses mainly due to valves V0 and V2 in Fig. 8. The head loss coefficient of one fully opened valve is about $K_v = \frac{2.4}{4^2/(2\times 9.8)} = 2.95$, which is high comparing to normal fully open butterfly valves [7].

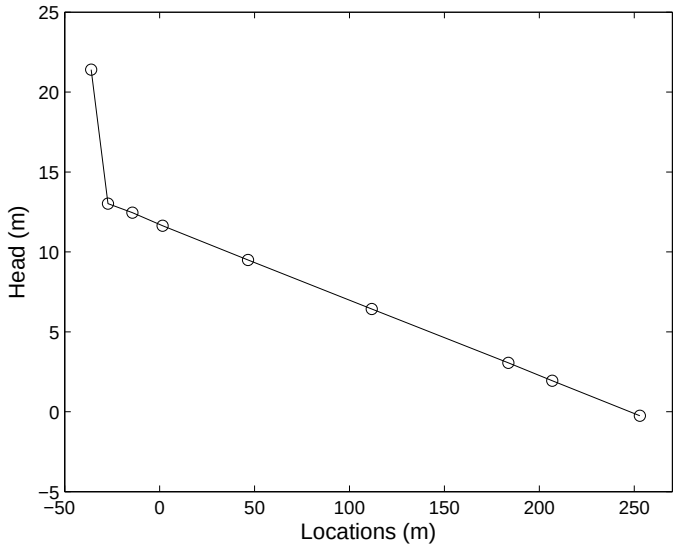

Figure 9: Hydraulic grade line for the entire pipeline.

4.2. Pipe filling

4.2.1. Inflow rate

The flow rates measured by the upstream and downstream flow meters are shown in Fig. 10. Without losing information, the early part of the outflow measurements is left out for clarity. Good repeatability is exhibited by three representative runs. The arriving time of the water front at the downstream flow meter ($x = 270.3$ m) is 54 ± 0.8 s. The area covered by the inflow rate curve between $t = 0$ and $t = 54$ s and the x-axis is the amount of water that has entered

the pipeline when the water front arrives at the downstream flow meter. The averaged value of this area is 11150 litres. It is less than the pipe volume $\forall = AL = \pi D_{PVC}^2/4 \times (270.3 + 6.5) \times 10^3 = 12047$ litres. The volume discrepancy is equivalent to a 20.6 m long PVC pipe. This implies that when the water column arrives at the downstream flow meter, not all air is expelled out of the system. This matter is further examined in next section.

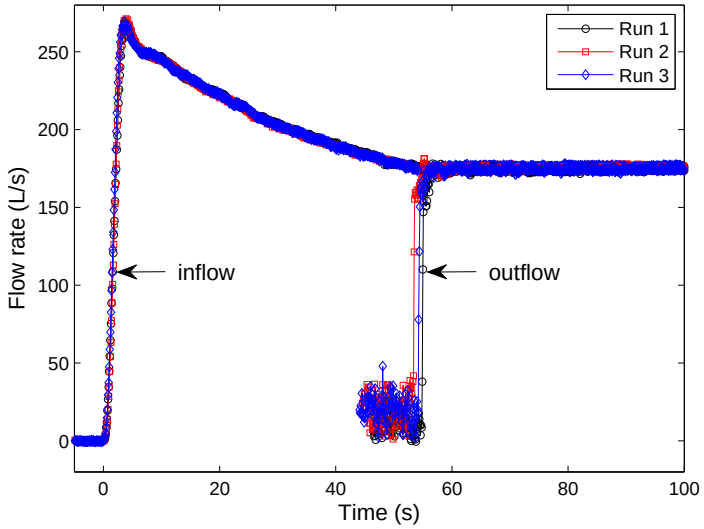

Figure 10: Measured inflow and outflow rates in three representative pipe filling runs.

Now we focus on the measurements by the upstream flow meter. As shown in Fig. 10, the flow rate first rises to its maximum value of 270 ± 3 L/s in about 4 seconds time. Then it experiences a rapid decreasing from 270 L/s to 250 L/s in 2 seconds time. After that, the flow gradually decelerates until a steady state is reached. The inflow velocity V – determined from the averaged flow rate of 9 runs – is shown in Fig. 11 by the solid line. The trend of the curve is the same as that in the small-scale experiments of Liou & Hunt [13]. The filling time is much longer (about 57 seconds) because of the large-scale. The measured maximum velocities are high (about 6.2 m/s) due to the 25 m high (relative to the inlet at $x = -34.6$ m) water tank driving the flow. The friction head loss at steady state in the whole system is about

$$h_f = f\frac{L}{D}\frac{V^2}{2g} = 0.0136 \times \frac{34.6 + 271}{0.2354} \times \frac{4^2}{2 \times 9.8} = 13.6 \text{ m}.$$

4.2.2. Water-air interface

Since the initial water front (water-air interface) splits into two water fronts during the filling process, the sketch in Fig. 12 is introduced for the sake of clearness. To determine the water front velocities V_1 and V_2, the measuring method of [13] is used. Two different groups of instruments are used as the front timing sections. The first group consists of the six water level meters (WL1, WL3, WL5, WL7, WL8 and WL9) located at $x = 1.7$, 46.4, 111.7, 183.7, 206.8 and 252.9 m. The second group consists of the pressure transducers (p_1, p_{3b}, p_5, p_7, p_8 and p_9) located at $x = 1.6$, 46.6, 111.7, 183.7, 206.8 and 252.8 m. Except for pressure transducer p_{3b} located at the pipe bottom, the other five transducers are in a horizontal plane with the pipeline axis. The water level meters are in a vertical plane with the pipeline axis. The arrival times of the advancing water fronts at the timing sections are captured by the two groups of instruments. The average speeds of the fronts are then computed from the distances between the timing sections and the travel times.

The determined water front velocities are shown in Fig. 11 by symbols; the squares indicate V_1 and the diamonds V_2. Note that the velocities V_1 and V_2 are averaged velocities over the trajectory between two subsequent sections. The location of the symbols indicate the arrival times of the water fronts at the timing sections. Only velocities determined from water level meters are presented in Fig. 11. This is because the pressure transducers gave results

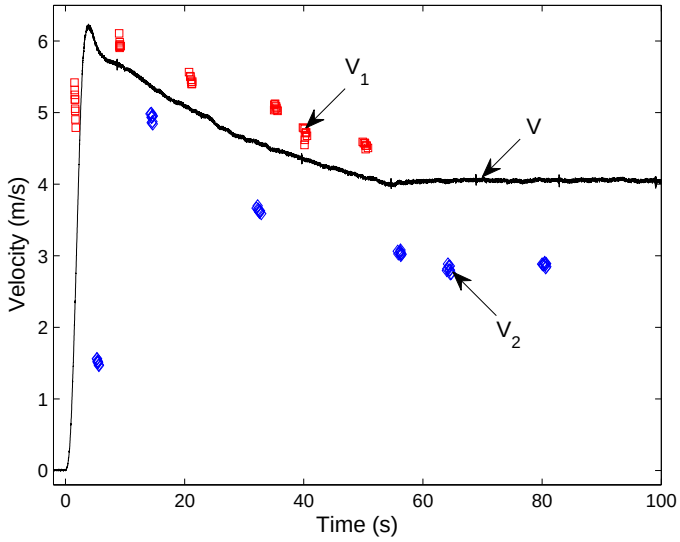

Figure 11: Velocity history of the inflow and the water column fronts in the filling experiments. Solid line – adapted from upstream EMF measurements; symbols – indirect measurements (squares – V_1 – leading front, diamonds – V_2 – secondary front).

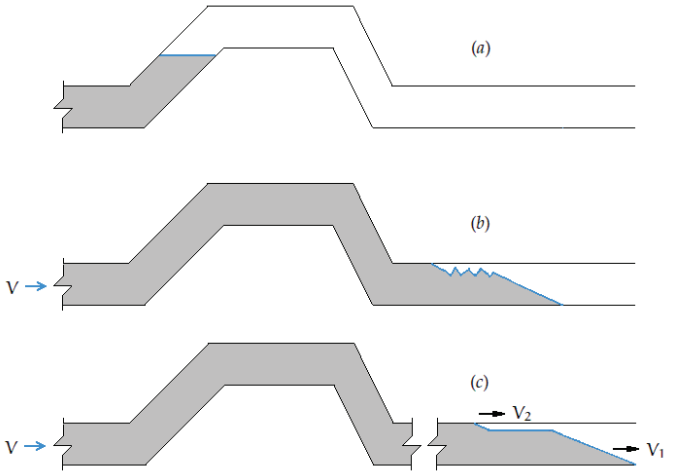

Figure 12: Water front evolution in the filling process – one original water front splitting into two fronts: (a) initial state, (b) early stage of filling and (c) forming of two water fronts.

close to that from the water level measurements for the leading front 1, whilst they could not accurately sense the arrival of the secondary front 2. The reason why the pressure transducers do not work well for detecting front 2 is the small pressure rise due to the arriving of water front 2. The water front starts from $x = -6.5$ m and has splitted into two fronts when it arrives at section 1 ($x = 1.7$ m). The overall trend of the velocities of both water fronts follows the inflow measurement. The timing sections, arrival times and water front velocities are listed in Tables 5 and 6. When water front 1 is travelling between section 3 ($x = 46.4$ m) and section 9 ($x = 252.9$ m), the velocity difference between V and V_1 is roughly 0.4 m/s, except at section 8 ($x = 206.8$ m) where it decreases to 0.24 m/s. Similarly, before water front 2 arrives at section 9, the velocity difference between V and V_2 is about 1 m/s except at section 8 ($x = 206.8$ m), where the difference increases to 1.25 m/s. The velocity variation at section 8 is because of a phenomenon like hydraulic jump in open channel flow occurred between sections 8 and 9 as shown below from the water level meter measurements.

Liou & Hunt [13] used the above method to measure the average velocity of the water column V, as there was

Table 5: Propagation of water front 1 in the filling process. The unit for x, t and V is m, s and m/s, respectively.

Section	x	t_1	V_1	V	$V_1 - V$
1	1.7	1.61± 0.07	5.09	2.61	2.48
3	46.4	9.12± 0.16	5.96	5.66	0.30
5	111.7	21.09± 0.36	5.46	5.05	0.41
7	183.7	35.28± 0.33	5.07	4.50	0.43
8	206.8	40.20± 0.35	4.70	4.36	0.24
9	252.9	50.34± 0.44	4.55	4.10	0.45

Table 6: Propagation of water front 2 in the filling process. The unit for x, t and V is m, s and m/s, respectively.

Section	x	t_2	V_2	V	$V - V_2$
1	1.7	5.44± 0.18	1.38	5.84	4.46
3	46.4	14.51± 0.25	4.92	5.30	0.38
5	111.7	32.48± 0.40	3.63	4.56	0.96
7	183.7	56.17± 0.59	3.04	4.00	0.96
8	206.8	64.39± 0.36	2.81	4.06	1.25
9	252.9	80.42± 0.41	2.87	4.03	1.16

no flow meter in their apparatus. In their experiment, at each timing section, two opposing metal pins were inserted radially in a horizontal plane (similar as the pressure transducers in our experiment), leaving an air gap between them. Upon the arrival of the front of the water column, the air gap closed and a voltage was generated. Consequently, their measured velocity was the velocity of water front 1 (V_1). Under the assumption that the filled pipe remains full (no air intrusion), the water front velocity V_1 is indeed the same as the inflow velocity V.

The water level meter measurements for three repeated runs are shown in Fig. 13. A good repeatability is seen again. The splitting of the water front is evident. The water levels in one typical run are shown in Fig. 14. As shown in Figs. 13 and 14, the pipeline is not entirely empty before a filling test. Water is mainly present between section 3 (x = 46.6 m) and section 8 (x = 206.8 m), and has the highest level 35 mm at section 5 (x = 111.7 m). This is because of the incomplete emptying before the filling test. The shown results are from the tests using 2 bar air pressure for emptying. When lower air pressures were used, more water stayed in the system. The evolution of the water front then becomes much more complex and the repeatability of the tests is much less.

Figure 14 indicates that the shape of water front 1 does not change much until it arrives at section 9 (x = 252.9 m). Its final length is about 3 metres as estimated from the rise time (0.5 – 0.75 s) and the measured velocity. The wedge-shaped front (see Figs. 14 and 12c) is mainly due to the pipe bridge. The average height of water front 1 is more or less constant (193 ± 8 mm) until it arrives at section 9 (x = 252.9 m) where it increases to 230 mm. Water front 2 reaches section 1 (x = 1.7 m) at about t = 5.4 s. Its shape slightly changes with time. The average height of water front 2 is approximately constant until it arrives at section 8 (x = 206.8 m). It decreases to 6 mm at section 9 (x = 252.9 m). The dramatic change of the height of the two water fronts indicates that a large flow regime transition (like a hydraulic jump) must have occurred between sections 8 (x = 206.8 m) and 9 (x = 252.9 m). The distance between the two water fronts lengthens with time. It is about 20 m when water front 1 arrives at x = 1.7 m (t = 1.6 s), and it increases to 75 m when water front 1 arrives at x = 206.8 m (t = 40.2 s). According to these observations, a quantitative analysis of the water-air interface evolution is sketched in Fig. 15.

The evolution of the water-air interface indicates the intrusion of air. When water front 1 has reached the pipeline end, the pipe at section 7 (x = 183.7 m) is still not full (see Fig. 14). The thickness of the air layer between the two water fronts is more or less constant before the occurrence of the hydraulic jump. The length of the air layer increases

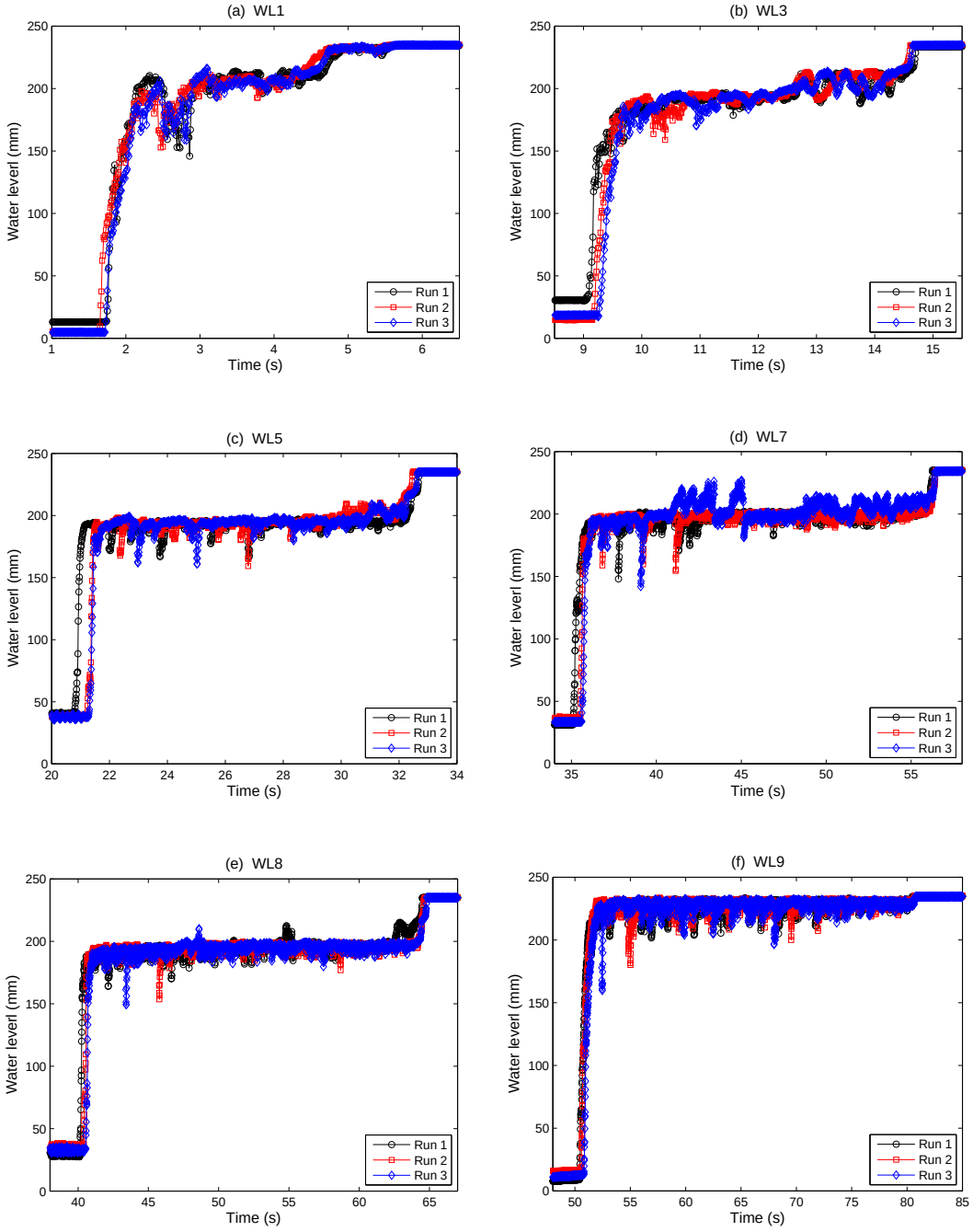

Figure 13: Water levels at six different locations in three repeated filling runs: (a) WL1, (b) WL3, (c) WL5, (d) WL7, (e) WL8 and (f) WL9. See Tables 1 and 5 for locations.

with time. That is, with the advancement of the water fronts, more air enters the water column from its top. This is consistent with the conclusion drawn from the flow rate measurement that the system is not full when the leading front arrives at the downstream flow meter.

Based on the heights of the water fronts shown in Figs. 13 and 15 and together with Fig. 11 and Tables 5 and

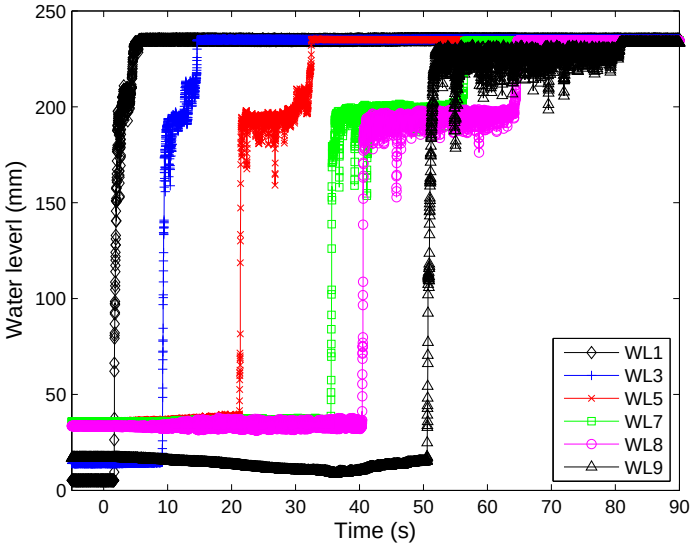

Figure 14: Water level changes at six different locations in one representative filling run.

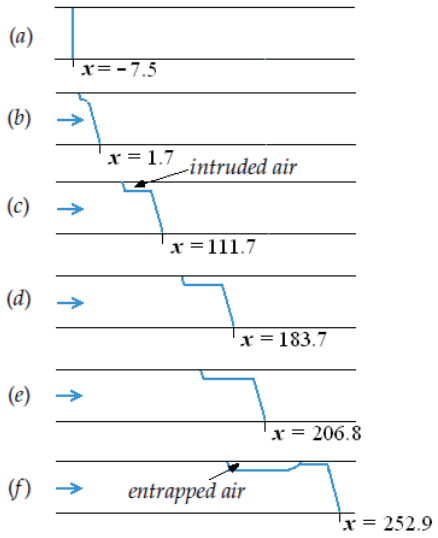

Figure 15: Illustration of air intrusion in the filling experiments (unit: m). The intruded air lengthens while its thickness does not change in stages (b), (c), (d) and (e). A phenomenon like hydraulic jump occurred between stages (e) and (f), after which entrapped air is gradually expelled from the system.

6, the conservation of volume at the moment (t = 21 s) that water front 1 arrives at section 5 (x = 111.7 m) is checked. The inflow rate is $Q_{in} = VA = 5.05 \times 0.0435 = 0.22$ m^3/s. The volume change at the water fronts is $Q_{out} = V_1A_1 + V_2A_2 = 5.46 \times 0.0381 + 4.5 \times 0.0054 = 0.23$ m^3/s. The areas A_1 and A_2 are obtained from the water level 192 mm. Velocity V_1 is taken from Table 5 and V_2 is interpolated from Table 6. Approximately Q_{in} equals Q_{out}. Thus the conservation of volume is verified.

The volume of the intruded air is also checked. When water front 1 arrives at x = 206.8 m (t = 40.2 s), the volume of the filled water (covering area of the flow rate curve between t = 0 and t = 40.2 s) is $\forall_1$ = 8700 litres. The initial voided pipe volume is $\forall_2 = LA = (206.8 + 6.5) \times 0.0435 \times 10^3 = 9275$ litres. Hence the volume of the intruded air is $\forall_{air} = \forall_2 - \forall_1 = 575$ litres. We used the measured water level (191 mm) to calculate $\forall_{air}$ too. The air volume on top of the stratified water platform is $0.0057 \times 10^3 \times 75 = 430$ litres. The air volume on top of the wedge-shaped

water front is about 100 litres (estimated from the length and the height of the wedge-shaped front). Consequently, the intruded air volumes calculated using the two approaches are more or less the same. The discrepancy is because of the oscillation of the stratified free surface (spikes in Fig. 13e). This verification confirms the water level measurements.

According to the gravity current theory of Benjamin [2], the height of the water front 1 for a steady current in horizontal tube of circular cross-section is $0.5625D_{PVC} = 132$ mm. It is 32 percent smaller than the measurement (195 mm) herein. This is because no steady state is achieved for the pressure driven flow in the filling process. In steady gravity current theory, the water front velocity equals the gravity wave celerity.

4.2.3. Pressure

Pressure histories at different locations along the PVC test pipeline are shown in Fig. 16. When the water column arrives at the downstream bend ($x = 267$ m) at $t = 54$ s, the recorded pressures show some oscillations due to impact. The magnitude of the oscillation at section 9 ($x = 252.9$ m) is 0.1 barg, which is approximately equal to $0.5\rho V_1^2 = 0.5 \times 1000 \times 4.5^2/10^5 = 0.1$ barg.

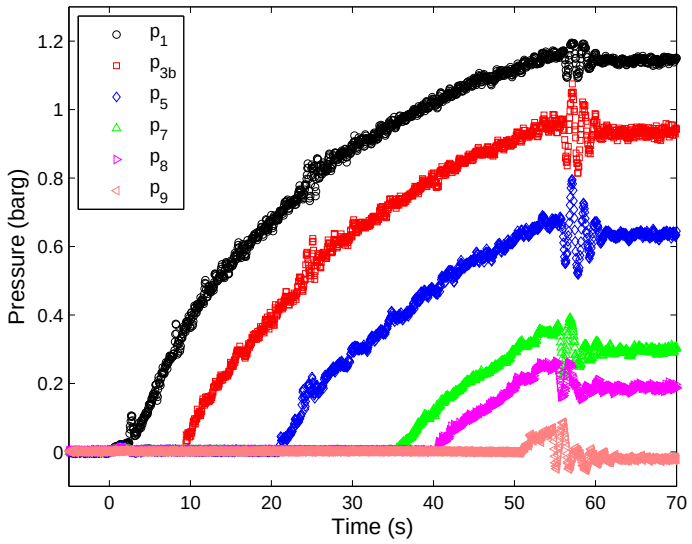

Figure 16: Pressure history at six different locations along the PVC test section in one typical run. See Table 1 for locations.

The pressure histories of transducers p_u ($x = -14$ m) and p_{uv} ($x = -27.7$ m) are shown in Fig. 17 together with p_1 ($x = 1.6$ m). At the beginning of filling, p_u and p_{uv} experience a rapid change (short lived peak for 3 seconds) and then gradually increase as p_1 does. The rapid change of p_u and p_{uv} may be attributed to the entrapped air between the T-junction ($x = -27.2$ m) and the check valve ($x = -43.1$ m). The peak in driving pressure can be part of the reason for the short-lived flow rate peak (see Fig. 11).

Comparing Fig. 16 with the water level measurements in Figs. 13 and 14, the intruded air on top of the stratified flow (see Fig. 15) is not under atmosphere. For example, the water level at section 5 ($x = 111.7$ m) is about 193 mm from $t = 21$ s to $t = 32$ s as shown in Fig. 13c, but pressure p_5 increases gradually during that time interval as shown in Fig. 18a. Similarly, as shown in Fig. 13e, the water level at section 8 ($x = 206.8$ m) is about 192 mm during the time interval between 40 s and 65 s. If the air on top is under atmosphere, the pressure head at section 8 should be smaller than $195 - D_{PVC}/2 \approx 77$ mm during that time interval. This is apparently different from the measurement of p_8 as shown in Fig. 18b. These demonstrate that the intruded air is under pressure higher than atmospheric. This is the reason why we referred to the water level change between sections 8 and 9 as a phenomenon like hydraulic jump in open channel flow. Due to the pressurized entrapped air, the hydraulic jump stayed in between sections 8 and 9. Vasconcelos *et al.* [24] used pressure transducer measurements to estimate the water level in their experiments by assuming that the air on top is under atmosphere (open channel flow). Although we cannot conclude that their

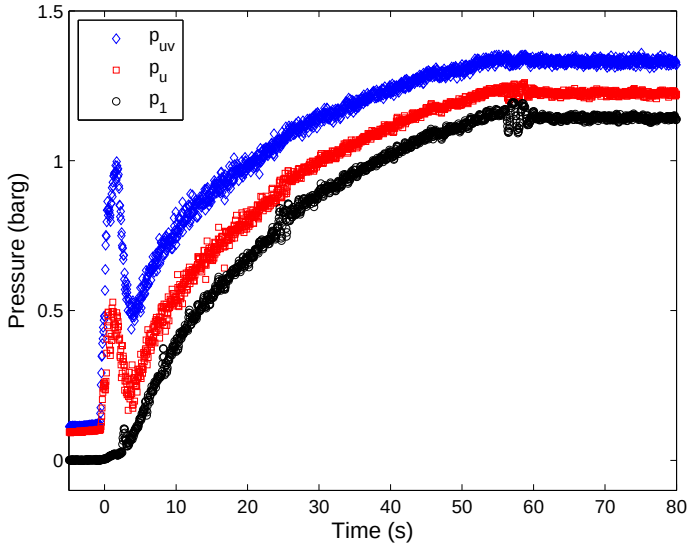

Figure 17: Pressure history at $x = -27.7$ m (p_{uv}) and -14 m (p_u) in a typical filling run.

treatment was wrong because a smaller diameter pipe ($D = 94$ mm) was used, it is suspicious to do that especially when stratified flow with a flat top forms.

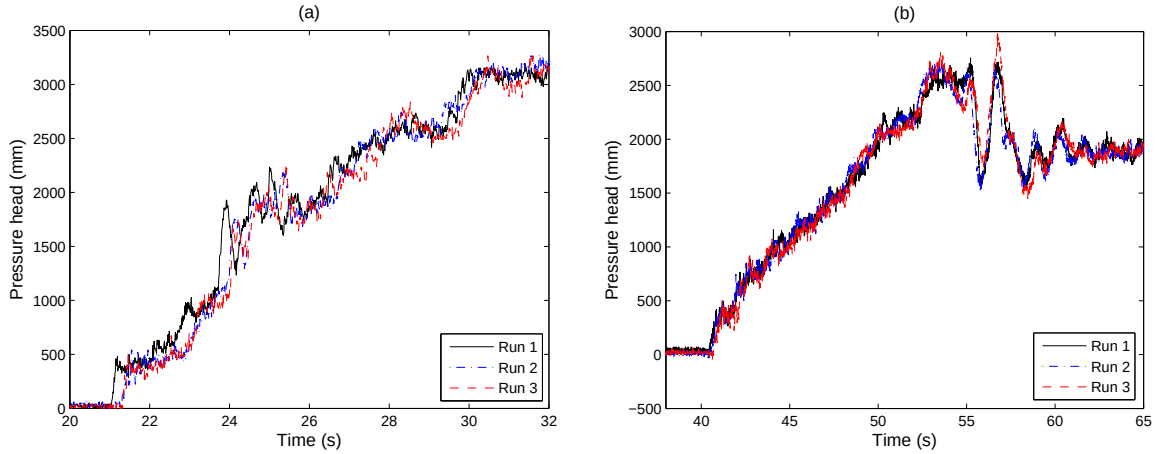

Figure 18: Pressure history at two locations along the PVC test section in three repeated filling runs: (a) section 5 ($x = 111.7$ m) and (b) section 8 ($x = 206.8$ m).

The pressure distribution (hydraulic grade line) at three time levels are shown in Fig. 19. The chosen times are the instants when water front 1 arrives at the transducers p_5 ($x = 111.7$ m), p_7 ($x = 183.7$ m) and p_9 ($x = 252.8$ m). The linear pressure distribution along the water column means a uniform pressure gradient decreasing in time. It implies that the advancing water column behaves like a rigid column, although air intrusion takes place. It also confirms the above observation of the non-atmospheric intruded air. This can be clarified as follows. When water front 1 arrives at section 9 ($x = 252.8$ m), water front 2 does not arrive at section 7 ($x = 183.7$ m) (see Fig. 14). If the air is under atmospheric pressure, the pressure distribution between sections 7 and 9 will be flat and close to zero. This is apparently not the case shown in Fig. 19.

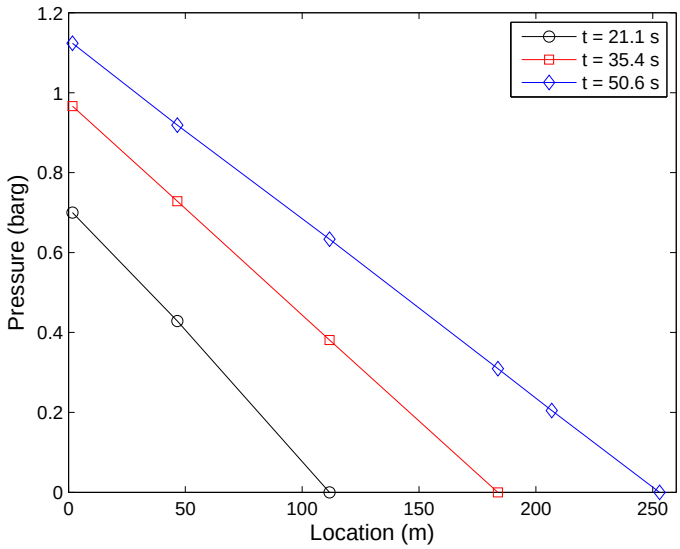

Figure 19: Pressure distribution along water column in the filling process at three time levels when water front 1 arrives at section 5 (x = 111.7 m) – circles, section 7 (x = 183.7 m) – squares, and section 9 (x = 252.9 m) – diamonds. The x-coordinates of the symbols are the locations of the pressure transducers.

4.3. Pipe emptying

4.3.1. Outflow rate

The outflow rates measured in different pipe draining test cases (see Table 2) are depicted in Figs. 20 – 32. The shown measurements are from rest to the instant when the leading air front (air-water interface) arrives at the outlet flow meter. Good repeatability is verified by three representative runs shown in Fig. 20. In all figures – out of five repetitions – the runs with the lowest and highest flow rates are shown and one "intermediate" run. Three cases where the repeatability is not well established are the cases 5, 9 and 13 as shown in Figs. 24, 28 and 32, respectively. They represent the more extreme conditions (case 5: draining under gravity only; cases 9 and 13: 2/9 opening of the downstream butterfly valve V4) and for the time being will not be further processed due to their lack of repeatability.

In the cases with a maximal open downstream valve (9/9-opening of valve V4 in cases 1 – 4; see Figs. 20 – 23), largely opened valve V4 (positions of 8/9-opening in cases 6 and 10; see Figs. 25 and 29) and intermediately opened valve V4 (positions of 5/9-opening in cases 7 and 11; see Figs. 26 and 30), the water column acceleration changed roughly in three stages. After the sudden opening of the downstream valve V5, the flow accelerated rapidly with water hammer from rest. Then followed a slowly increasing discharge (more or less linear). Before the air-water front visibly and audible flushed out from the outlet, a second rather rapid flow acceleration occurred. In the cases with a largely closed valve V4 (with open positions of 4/9 in cases 8 and 12), the second rapid acceleration is absent (see Figs. 27 and 31).

The maximum difference between 3 repetitions of the emptying time is about 2.5 seconds (see Fig. 21), and the maximum flow rate difference is about 20 L/s (see Fig. 26) relative to 300 L/s outflow rate. The detailed information is listed in Table 7. The arrival time is the instant that the leading air front arrives at the downstream flow meter. It is designated as t_d (drainage time). The maximum value of the standard deviation, determined for all valid cases, is less than 3.4 percent. Similar to pipe filling, the area covered by the outflow rate curve from $t = 0$ until $t = t_d$ and the x-axis is the volume V_d of water driven out of the system. The volume of the initial water in the pipeline between the check valve ($x = -43.1$ m) and the downstream flow meter ($x = 270.3$ m) is about $\forall = L_1A_1 + L_2A_2 + L_3A_3 = (29.1 \times 0.0296 + 275.2 \times 0.0435 + 9.1 \times 0.0437) \times 10^3 = 13230$ litres. The integrated drainage $\forall_d$ is presented in Table 7. When valve V4 is fully open, the drainage at t_d increases with the driving air pressure. For a given driving air pressure, the drainage decreases with reducing of the opening of valve V4. The averaged volume V_d of the expelled water is 10309 ± 498 L. Apparently, not all the expected water is driven out of the system at time t_d. It implies that the initial planar air-water interface has stratified during draining. This becomes more clear from the water level meter

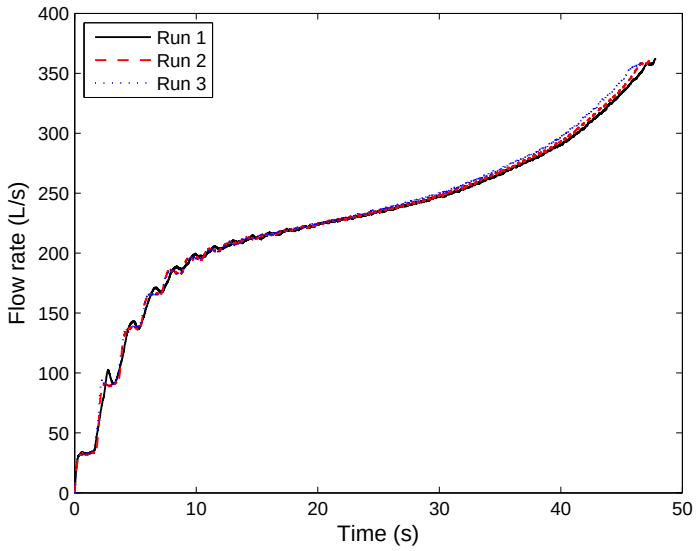

Figure 20: Outflow rate in the emptying experiment. Case 1: 2.0 barg initial air-circuit pressure and 9/9 opening of valve V4.

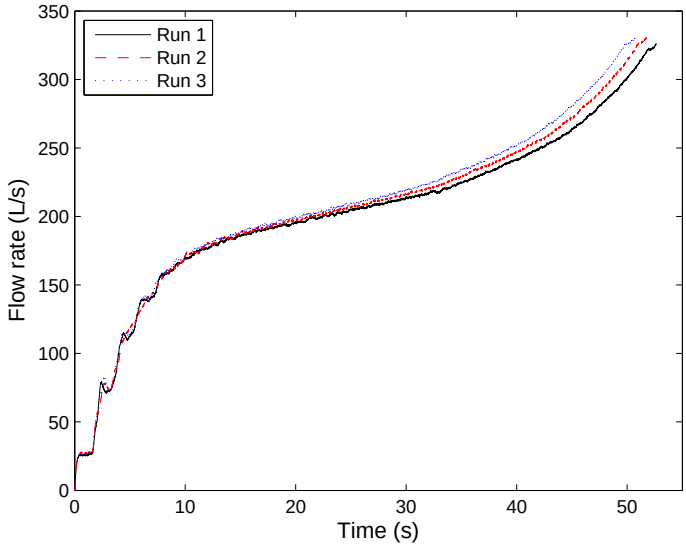

Figure 21: Outflow rate in the emptying experiment. Case 2: 1.5 barg initial air-circuit pressure and 9/9 opening of valve V4.

measurements examined below. With respect to case 1, the volume of the remaining water is equivalent to a 55 m long PVC pipe. When the remaining water is assumed to locate between section 3 (x = 46.4 m) and the downstream bend (x = 267 m), its level is about 70 mm. It is higher than the water levels observed in Fig. 14, because the emptying (after t_d) continues with some water slugs (see water level measurements in next section).

To show the effect of the driving air pressure p_{air} and the resistance of valve V4, ten typical flow-rate curves for the ten cases are presented in Fig. 33. Intuitively, flow with 1.0 barg driving pressure and 4/9-opening of valve V4 (case 12) should have the lowest flow rate and thus the slowest emptying process, while flow with the highest driving air pressure (2 barg) and the largest opening of valve V4 (9/9-opening) (case 1) should result in the highest flow

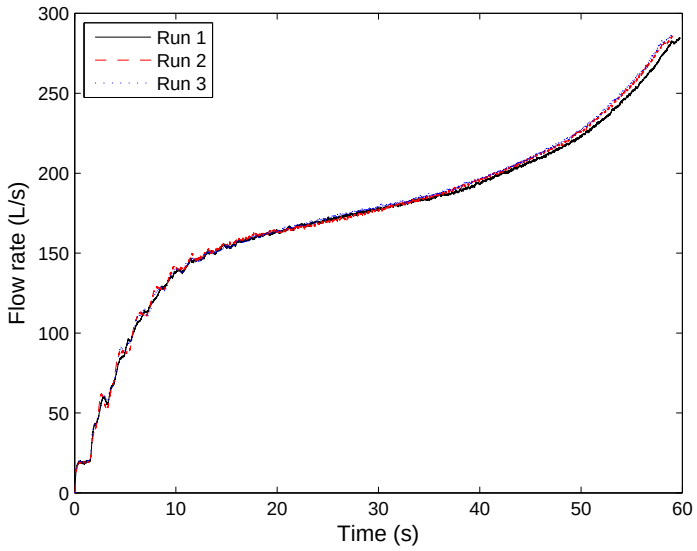

Figure 22: Outflow rate in the emptying experiment. Case 3: 1.0 barg initial air-circuit pressure and 9/9 opening of valve V4.

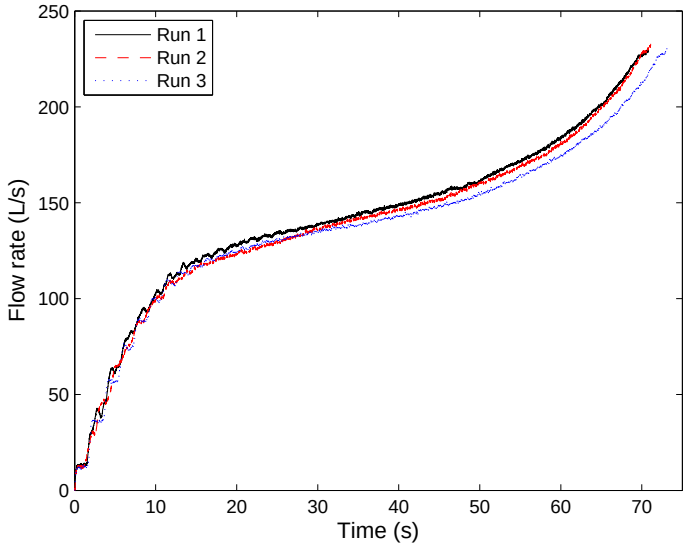

Figure 23: Outflow rate in the emptying experiment. Case 4: 0.5 barg initial air-circuit pressure and 9/9 opening of valve V4.

rates and consequently the most rapid emptying process. The first guess is obviously correct as shown in Table 7 and Fig. 33. But next to case 1 the flow in case 6 (p_a = 2 barg, 8/9-opening of valve V4) has the largest flow rates and shortest emptying time. This may be attributed to the resistance characteristics of the downstream butterfly valve V4, i.e. 8/9 is more or less fully open, as can also be seen from cases 3 and 10.

The flow rate increases more quickly with a higher driving pressure as shown in Fig. 34 with respect to full opening of valve V4. For other partial valve openings (8/9-, 6/9- and 4/9-opening), similar trends are observed. With a given driving pressure, the flow rate decreases with the reducing of the valve opening as shown in Fig. 35 (p_a = 2.0 barg) and Fig. 36 (p_a = 1.0 barg).

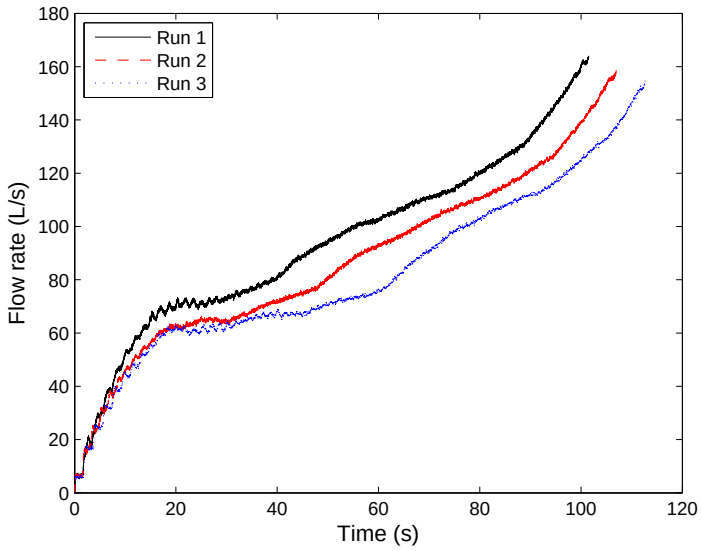

Figure 24: Outflow rate in the emptying experiment. Case 5: 0 barg initial air-circuit pressure and 9/9 opening of valve V4.

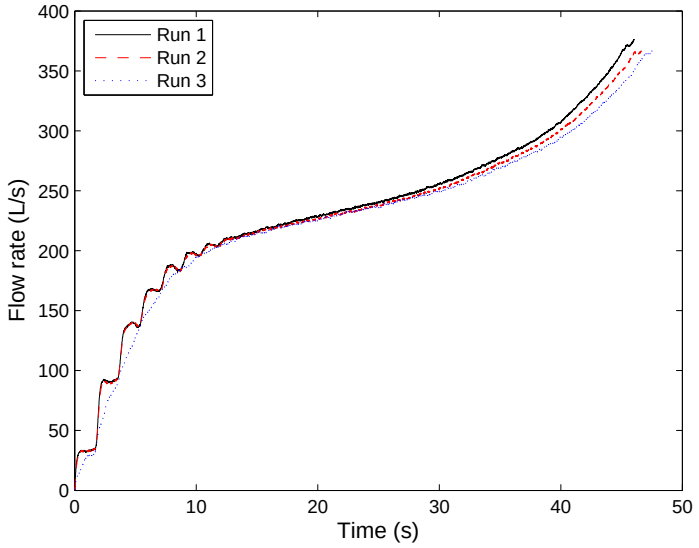

Figure 25: Outflow rate in the emptying experiment. Case 6: 2.0 barg initial air-circuit pressure and 8/9 opening of valve V4.

For the sake of convenience, the valid 10 test cases are classified into three groups according to the magnitudes of the outflow rates. The first group includes cases 1, 2, 6 and 7, of which the magnitudes are higher than 300 L/s (velocity is higher than 6.9 m/s). The second group includes cases 3, 4, 10 and 11, of which the final magnitudes are higher than 200 L/s (velocity is higher than 4.6 m/s). The last group includes cases 8 and 12, of which the flow rates are lower than 200 L/s. The three groups are referred to as violent, intermediate and gentle emptying, respectively.

The measurements of the upstream EMF for the different test cases are also examined. It is found that there is a time difference between the start time of the two EMFs (see Fig. 37). The time difference is approximately the water hammer wave travelling time (L/c) in the water column. Before the leading air front passes the upstream EMF, the

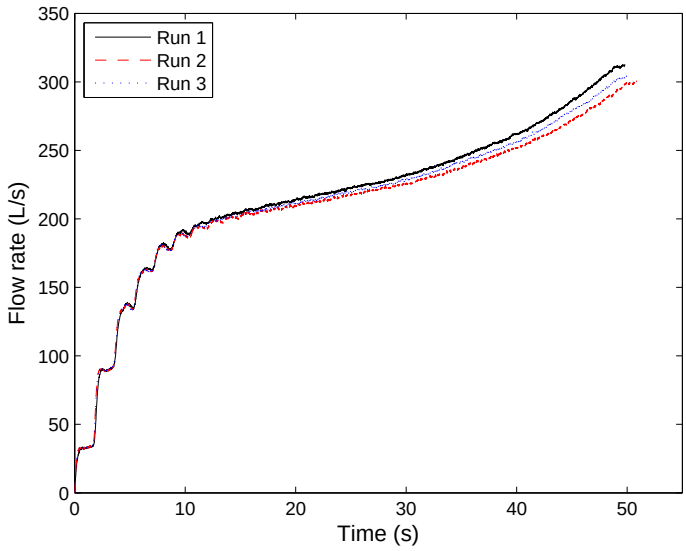

Figure 26: Outflow rate in the emptying experiment. Case 7: 2.0 barg initial air-circuit pressure and 6/9 opening of valve V4.

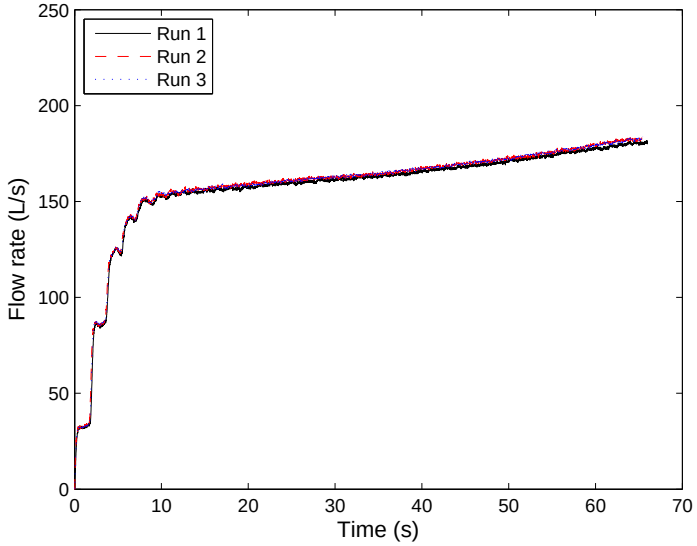

Figure 27: Outflow rate in the emptying experiment. Case 8: 2.0 barg initial air-circuit pressure and 4/9 opening of valve V4.

measured flow-rate curve shows the same trend as that of the downstream EMF (more or less parallel but without fluctuations).

4.3.2. Air-water interface

During emptying, the original planar (vertical) front (air-water interface) becomes stratified, forming a main air front and a ”hold-up”. For clearness, the sketch for the air front evolution during draining is shown in Fig. 38. It is different from the evolution of the water-air interface in pipe filling (see Fig. 15).

To determine the velocity of the main air front, the water level meters are used again as the timing points. Pressure transducers are not used because it is difficult to accurately determine the arriving time of the air due to much noise.

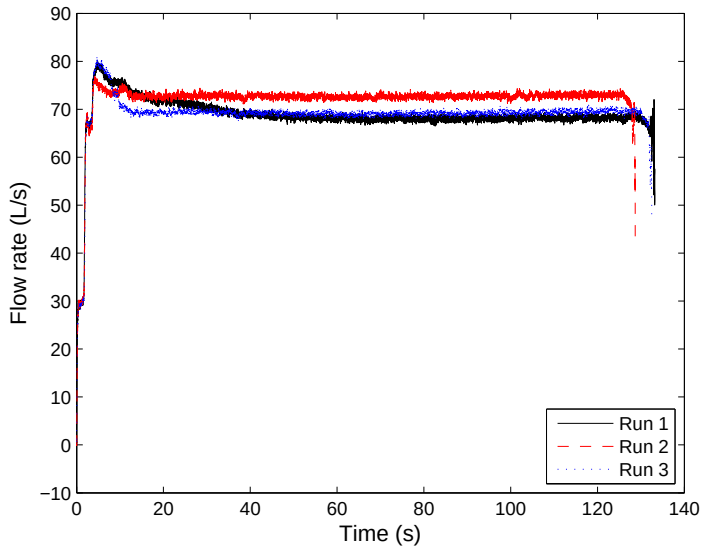

Figure 28: Outflow rate in the emptying experiment. Case 9: 2.0 barg initial air-circuit pressure and 2/9 opening of valve V4.

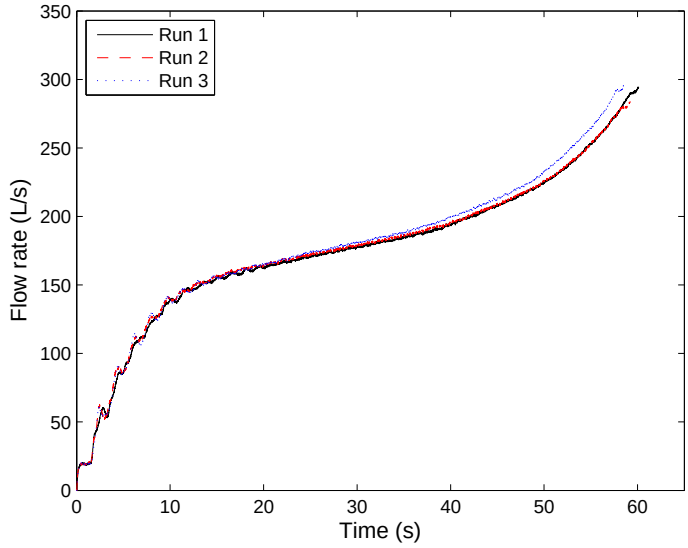

Figure 29: Outflow rate in the emptying experiment. Case 10: 1.0 barg initial air-circuit pressure and 8/9 opening of valve V4.

The results for the six representative cases 1, 2, 6, 7, 10 and 11 are shown in Figs. 39 – 44. The location of the dots indicate the arrival times of the leading air front at the timing sections. They have the same trend as the outflow-rate curves.

The velocity differences between the outflow and the main air front are listed in Table 8. The difference during large acceleration periods – air front arrives at section 1 (x = 1.7 m) and section 8 (x = 206.8 m) – is about 1 m/s for the examined six cases. During the ”linear” acceleration period, the velocity difference is more or less constant (about 0.75 m/s). At the late stage of emptying (the air front is at section 9 (x = 252.8 m)), the averaged velocity difference is 0.83 m/s. According to the gravity current theory [2] in tube emptying, the celerity of the air front, i.e. relative

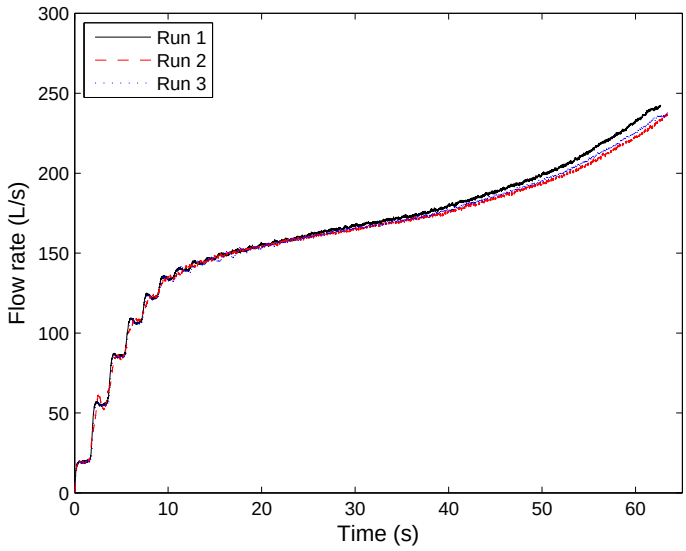

Figure 30: Outflow rate in the emptying experiment. Case 11: 1.0 barg initial air-circuit pressure and 6/9 opening of valve V4.

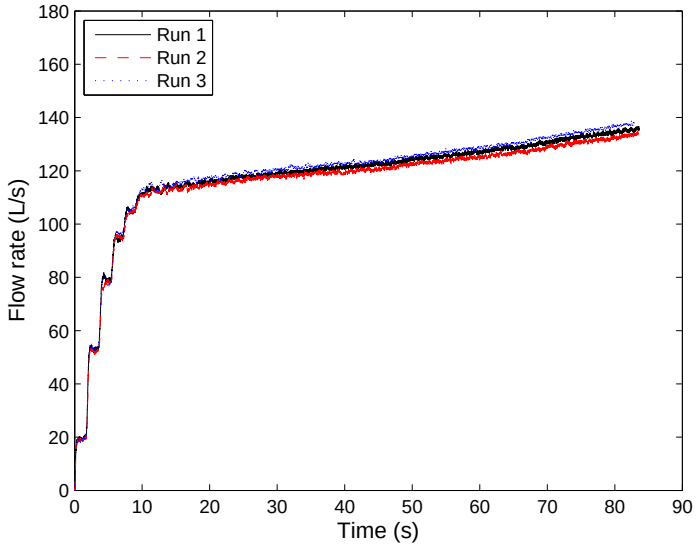

Figure 31: Outflow rate in the emptying experiment. Case 12: 1.0 barg initial air-circuit pressure and 4/9 opening of valve V4.

velocity to the steady water flow (upstream static fluid), is $c_{air} = 0.5\sqrt{gD_{PVC}} = 0.76$ m/s. It is very close to the relative velocity during the linear acceleration stage. In the experiments on long bubble motion of Zukoski [29], the btubble velocity in a one-meter horizontal tube is $0.76\sqrt{gD/2}$ for $D = 178$ mm and equals $0.65\sqrt{gD/2}$ for $D = 54.9$ mm. If they are used for the current experiment, the bubble velocity equals to $0.81\sqrt{gD_{PVC}/2} = 0.87$ m/s (0.81 is an extrapolated value), which is 16 percent higher than 0.75 m/s (quasi-steady state). This indicates that the observed long bubble motion in [29] is under rapid flow regime transition, but not a steady-state case as studied by Benjamin [2].

The water level meter measurements in case 6 (most violent flow in group 1) are shown in Fig. 45. For clearness

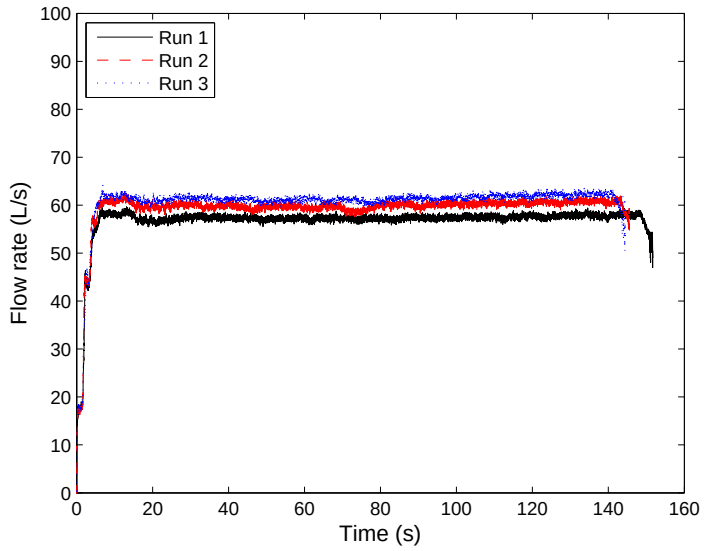

Figure 32: Outflow rate in the emptying experiment. Case 13: 1.0 barg initial air-circuit pressure and 2/9 opening of valve V4.

Table 7: Evolution of the leading air front in the emptying process. The unit for p_{air}, t_d, Q_{max} and $\forall_d$ is barg, s, L/s and L, respectively.

Case	p_{air}	ϕ	t_d	Q_{max}	$\forall_d$
1	2.0	9/9	47.24± 0.59	361.24 ± 1.08	10807
2	1.5	9/9	51.96± 1.22	330.07 ± 3.90	10597
3	1.0	9/9	59.21± 0.57	285.99 ± 0.96	10321
4	0.5	9/9	71.96± 1.19	230.90 ± 4.02	10027
6	2.0	8/9	46.56± 1.10	372.64 ± 4.17	10783
7	2.0	6/9	50.28± 0.60	307.18 ± 6.50	10680
8	2.0	4/9	65.66± 0.33	183.25 ± 1.38	10349
10	1.0	8/9	59.11± 1.01	293.75 ± 9.74	10381
11	1.0	6/9	63.19± 0.50	239.54 ± 3.17	10317
12	1.0	4/9	83.43± 0.48	137.16 ± 1.75	9811

Table 8: Velocity differences between the outflow and the leading air front in the emptying process. It is also the air intrusion velocity relative to the outflow (Unit: m/s).

Case \ x (m)	1.7	46.4	111.7	183.7	206.8	252.9
1	0.98	0.74	0.78	0.74	1.01	0.82
2	1.05	0.74	0.76	0.71	1.02	0.81
6	1.00	0.71	0.74	0.74	1.04	0.84
7	0.99	0.77	0.73	0.71	0.98	0.79
10	1.03	0.75	0.76	0.77	1.05	0.87
11	1.01	0.74	0.78	0.76	0.98	0.82

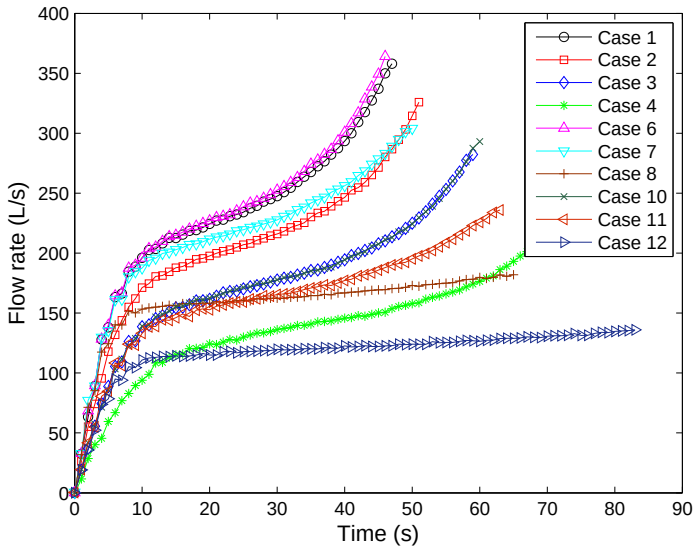

Figure 33: Outflow rates in the emptying experiment for 10 different conditions (Table 2. The time duration of the extracted data is from the opening of downstream valve at $t = 0$ s to the instant t_d when the main air front passes the downstream flow meter.

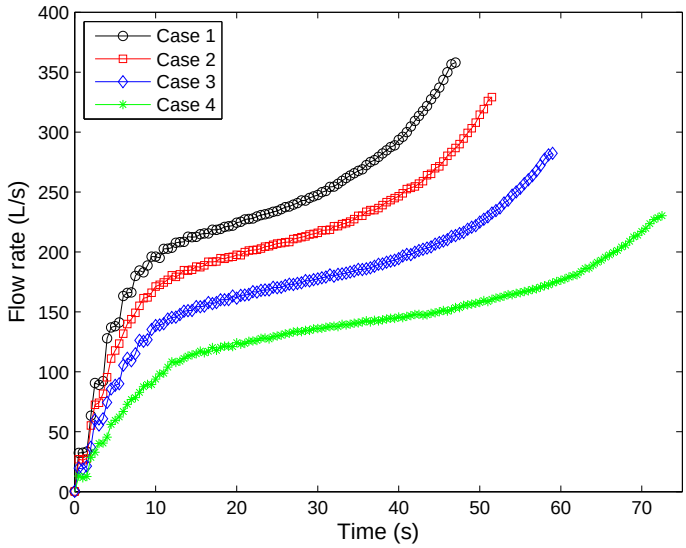

Figure 34: Outflow rates in the emptying experiment with fully open valve (9/9-opening) and different driving air pressures (2.0, 1.5, 1.0 and 0.5 barg).

the time interval between two points is 0.25 s. Behind the main air front, a water "tail" known as "hold-up" in normal slug flow (see Chapter 6) is formed. That is, with compressed air flowing in from upstream, not all water initially filling in the system is immediately flushed out. This is consistent with the observation from Table 7 and Figs. 39 – 44. After the passing of the air front, the "tail" at section 1 ($x = 1.7$ m) is small (about 10 mm deep) and the air-water interface is almost planar. At the other sections, the "tail" is thicker, e.g. about 100 mm at $x = 46.6$ m. The other three cases in group 1 confirmed this flow regime transition (stratification). The development of the water "tail" is because of gravity, turbulence and pipe skin friction. The water level change of the "hold up" after $t = 45$ s is because

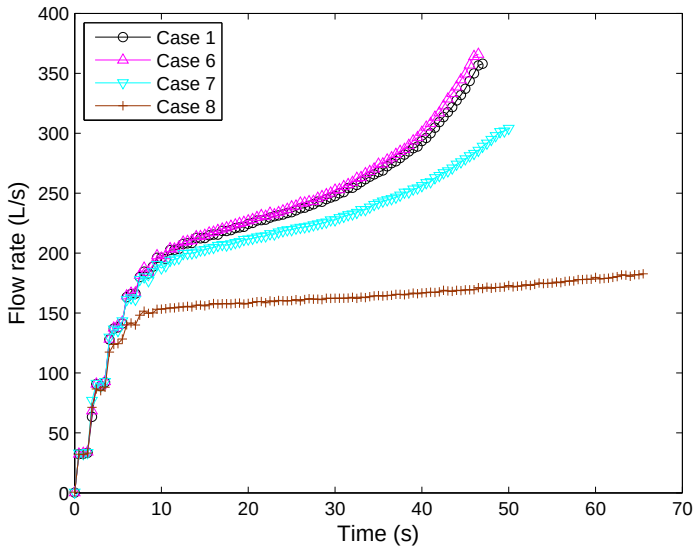

Figure 35: Outflow rates in the emptying experiment with fixed driving air pressure (2.0 barg) and different downstream valve openings (9/9-, 8/9-, 6/9- and 5/9-opening).

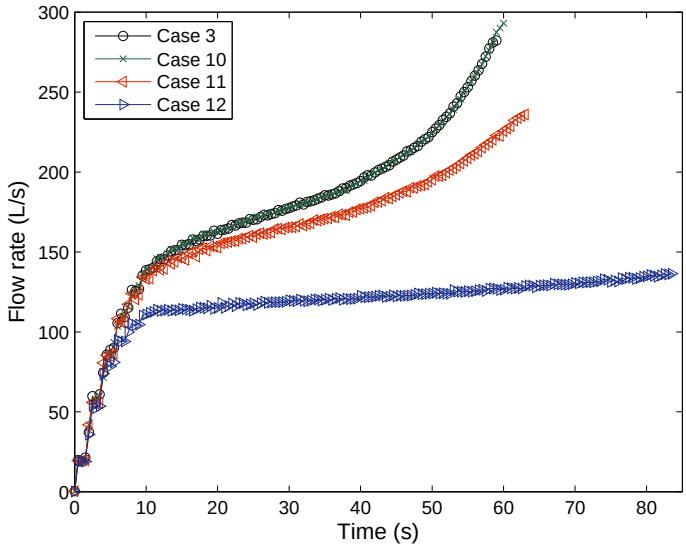

Figure 36: Outflow rates in the emptying experiment with fixed driving air pressure (1.0 barg) and different downstream valve openings (9/9-, 8/9-, 6/9- and 5/9-opening).

of the formation of slugs. The water level increase at section 1 after $t = 45$ s may be because of the flow returning from the 180 degree long bend. Another possible contribution is the flushing of the water remaining ahead of the pipe bridge. Its thickness is about 20 mm. Figures 46 and 47 show the water level meter measurements for cases 10 and 12, which represent the intermediate cases of group 2 and the gentle cases of group 3, respectively. Similar trends as in the violent case are observed. The only difference is the ”tail” thickness as shown in Figs. 45 – 47.

By taking case 6 as an example, the volume of the remaining water is checked. When the leading air front arrives at section 8 ($x = 206.8$ m) at $t = 40.2$ s (see Fig. 41), the volume of the expelled water (area integral of the outflow

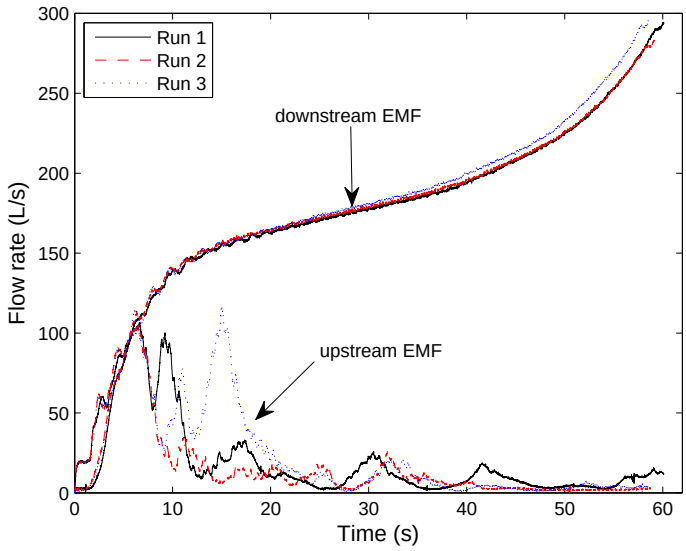

Figure 37: Flow rate measurements of the upstream and downstream flow meters in the emptying experiment (case 10).

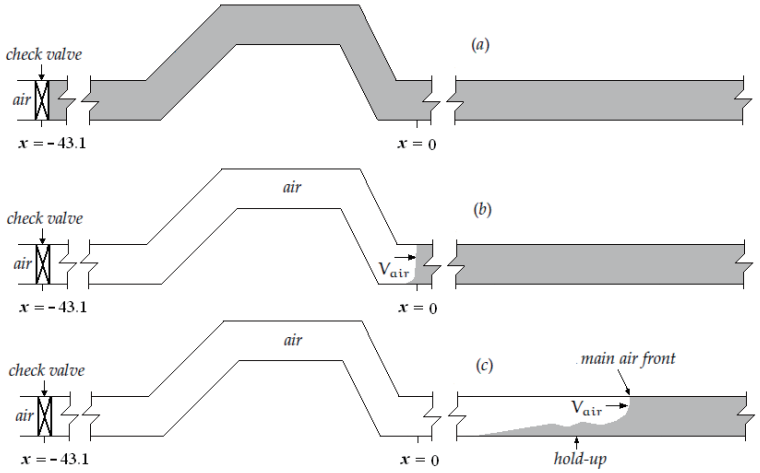

Figure 38: Illustration of air intrusion in the emptying experiments (unit: m). The air forms a main front and water hold-up behind it.

rate curve between $t = 0$ and $t = 40.2$ s in Fig. 25) is $\forall_1 = 8585$ litres. The volume of the initially filled water is $\forall_2 = L_1A_1 + L_2A_2 = [29.1 \times 0.0296 + (14 + 206.8) \times 0.0435] \times 10^3 = 10466$ litres. Hence the volume of the remaining water is $\forall_{rw} = \forall_2 - \forall_1 = 1881$ litres. We can also calculate $\forall_{rw}$ using the measured water levels at $t = 40.2$ s. From Fig. 45, the water levels at sections 3, 5, 7 and 8 is close to a constant 65 mm. The water level is 6 mm at section 1. We assume that the stratified flow starts from the middle of sections 1 and 3, i.e. $x = 22.4$ m with level of 65 mm. Then the volume of the remaining water is $(206.8 - 22.4) \times 0.0098 \times 10^3 = 1808$ litres. The volumes of the remaining water calculated using the two approaches are approximately the same (relative difference is 4 percent). This confirms the accuracy and consistency of the measurements in pipe emptying tests.

The conservation of volume at the moment ($t = 37$ s) when the leading air front arrives at section 7 ($x = 183.7$ m) is also checked. The outflow velocity reading from Fig. 41 is 6.45 m/s. The velocity of the leading air front is 7.19 m/s. The level of the water tail (stratified flow) is about 58 mm which is averaged from the water levels at sections (see Fig. 45) and hence the cross-sectional area of the tail is 0.0083 m^2. The outflow rate is $Q_{out} = VA = 6.45 \times 0.0435 =$

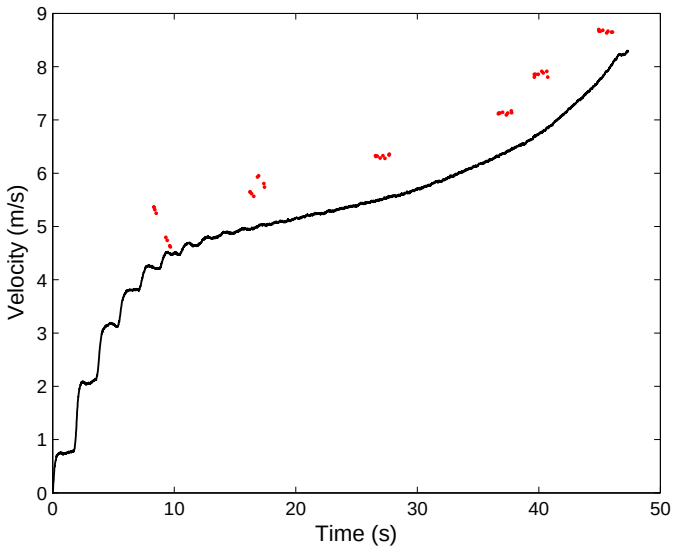

Figure 39: Velocity history of the outflow (solid line) and the main air front (dots) in the emptying experiments (case 1).

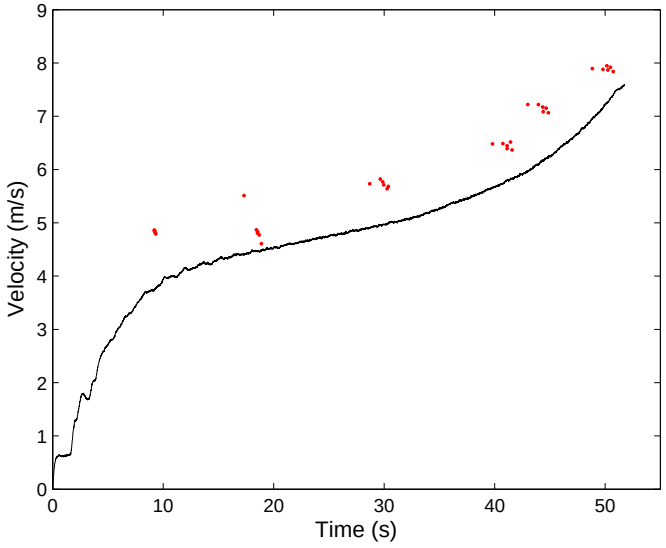

Figure 40: Velocity history of the outflow (solid line) and the main air front (dots) in the emptying experiments (case 2).

0.281 m^3/s. The air flow rate at the leading water front is $Q_a = V_a A_a = 7.19 \times 0.0352 = 0.253$ m^3/s. The difference between Q_{out} and Q_a is attributed to the movement of the water tail.

4.3.3. Pressure

The pressure measurements for the three representative cases 6, 10 and 12 are shown in Figs. 48 – 50. The pressure oscillations within the first 20 seconds are due to water hammer caused by the fast opening of the valve. For the violent and intermediate cases (cases 6 and 10), the water-pressure variations are characterized by a concave-up increase, until air arrives at the measurement sections. For the gentle case (case 12), the curvature is insignificant and the water-pressure increases more or less linearly. After some time, when the air front propagates through the

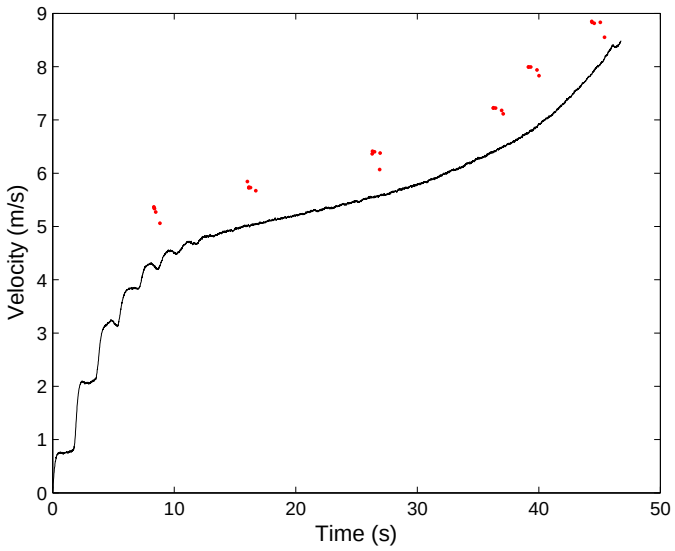

Figure 41: Velocity history of the outflow (solid line) and the main air front (dots) in the emptying experiments (case 6).

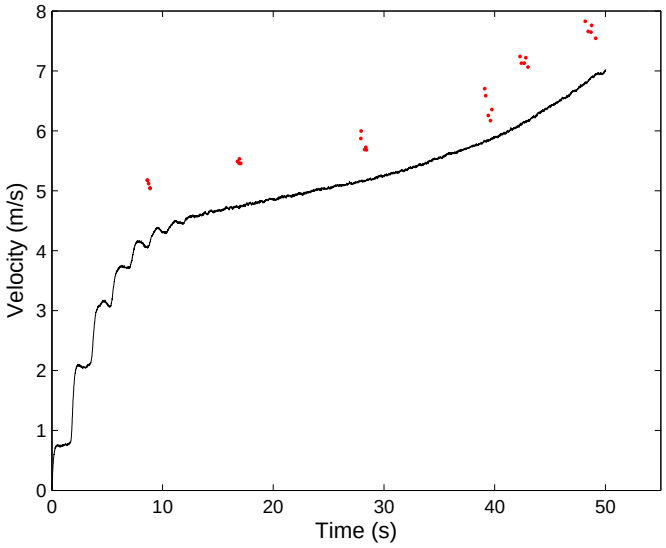

Figure 42: Velocity history of the outflow (solid line) and the main air front (dots) in the emptying experiments (case 7).

downstream end, impact of water slugs at the downstream bend causes pressure surges from the end of the pipeline up to section 7 (x = 183.7 m). Due to the large forces exerted by the water slugs, the downstream bend had large visible movements. The number of slugs varied from 2 to 4 for the three different cases. After the air front passes a section, the pressure at that place equals the driving air pressure. Consequently, the driving air pressure decreases more or less linearly in time during emptying. This is confirmed from the recordings of p_{air} at $x = -46.5$ m. The pressure change has similar shape as the velocity variation shown in Fig. 25.

From the pressure history at section 9 in case 6 (see Fig. 51), the Joukowsky pressure drop, i.e. $\Delta P = \rho c \Delta V$, is checked. The initial pressure decrease is 2.5 bar. The corresponding velocity change is 0.75 m/s as shown in Fig. 41.

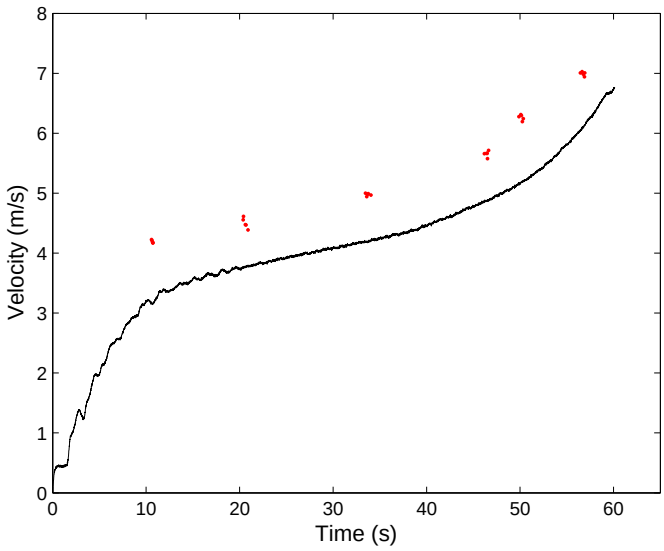

Figure 43: Velocity history of the outflow (solid line) and the main air front (dots) in the emptying experiments (case 10).

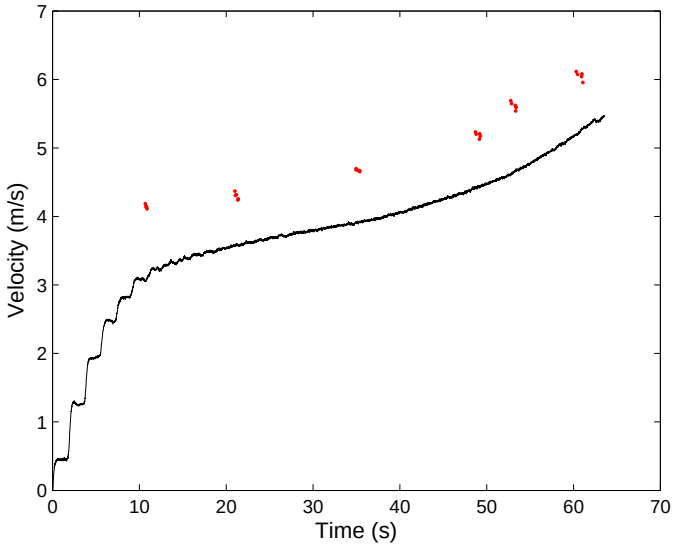

Figure 44: Velocity history of the outflow (solid line) and the main air front (dots) in the emptying experiments (case 11).

Accordingly, the pressure variation due to the velocity change is $\Delta P = \rho c \Delta V = 1000 \times 348 \times 0.75 = 2.61$ bar. The speed of sound $c = 348$ m/s is obtained from the water hammer tests [5]. This agrees well with the observed pressure change (the difference is about 5 percent). With the shortening of the water column, the pressure amplitudes becomes smaller and smaller. After about 12 seconds, the water-hammer event has been damped out. The pressure then smoothly increases.

The pressure distributions along the moving water column at the instant when the air front arrives at section 5 ($x = 111.7$ m) and section 7 ($x = 183.7$ m) are shown in Fig. 52. The straight "hydraulic grade line" means a constant pressure gradient and a rigid column. With the shorting of the water column, pressure at section 9 ($x = 252.9$ m)

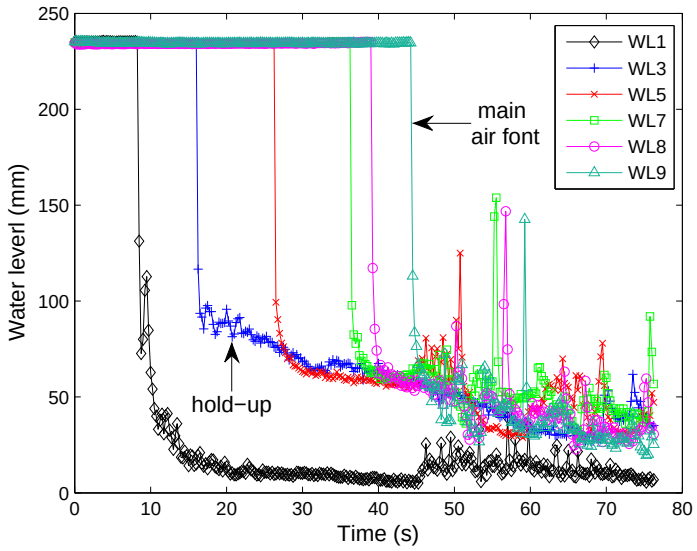

Figure 45: Water levels at six different locations along the PVC pipeline in the emptying experiments for the most violent case (case 6).

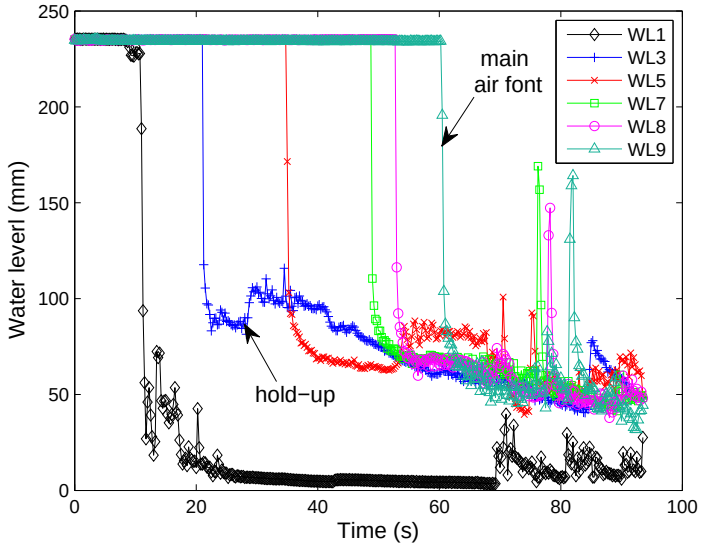

Figure 46: Water levels at six different locations along the PVC pipeline in the emptying experiments for the intermediate case (case 10).

increases. Similar observations are made for cases 10 and 12.

5. Numerical simulation

This section briefly reviews the mathematical modelling and gives some preliminary numerical simulations. For the modelling of the rapid filling of pipelines, the rigid-column theory based on a set of ODEs is commonly used. The rigid-column filling model for pipes in series was formulated in [13]. The model describes the unsteady motion of a lengthening water column filling empty pipelines with an undulating elevation profile. As shown in [1], by

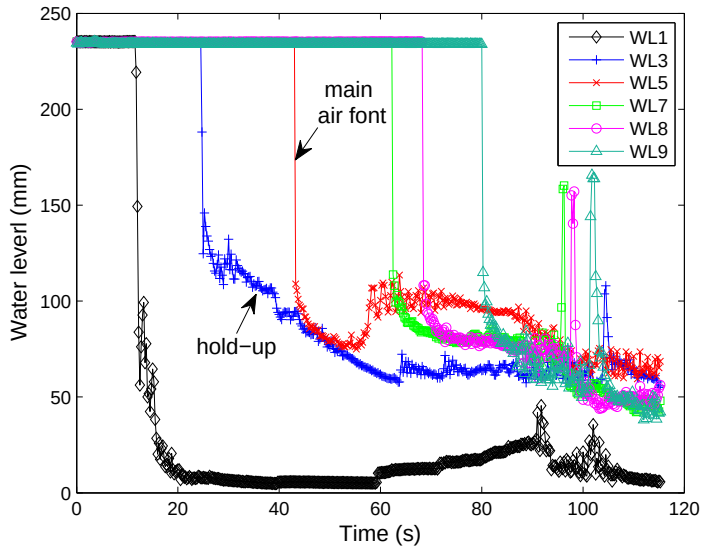

Figure 47: Water levels at six different locations along the PVC pipeline for the emptying experiments in the gentle case (case 12).

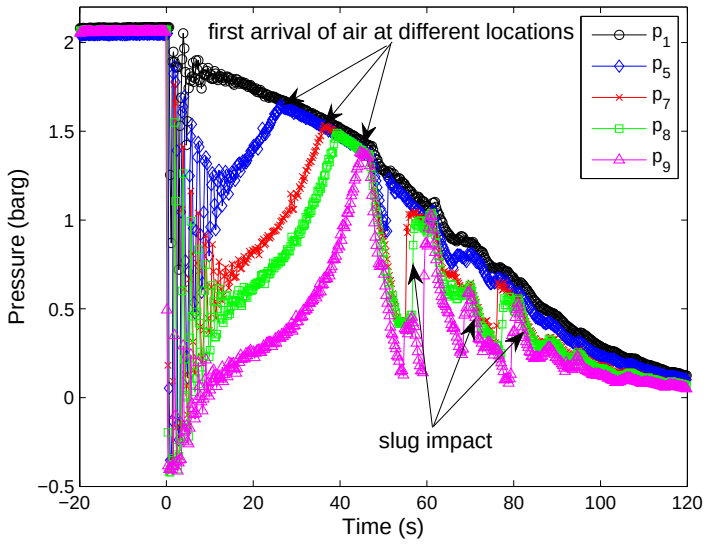

Figure 48: Pressure history at five different locations along the PVC pipeline in the emptying experiments for the most violent case (case 6).

decoupling the momentum equation from the pressure head at the pipe segment junctions, the filling process can be more efficiently calculated. The rigid-column model with the decoupling technique was recently extended to represent a branched system with undulating pipe segments [19]. By coupling the rigid-column model with an entrapped air model, Cabrera *et al.* [6] addressed filling pipes initially with air entrapped between water columns. The rigid-column model gives good results as long as the flow remains axially uniform. When the water column is disturbed somewhere in the system, pressure oscillations along its length or even column separation may result and then the rigid-column model will fail. Therefore, the elastic model based on a set of PDEs for unsteady flow in conduits (water-hammer equations with moving boundaries) was applied to simulate the rapid filling process [15]. This model is capable of

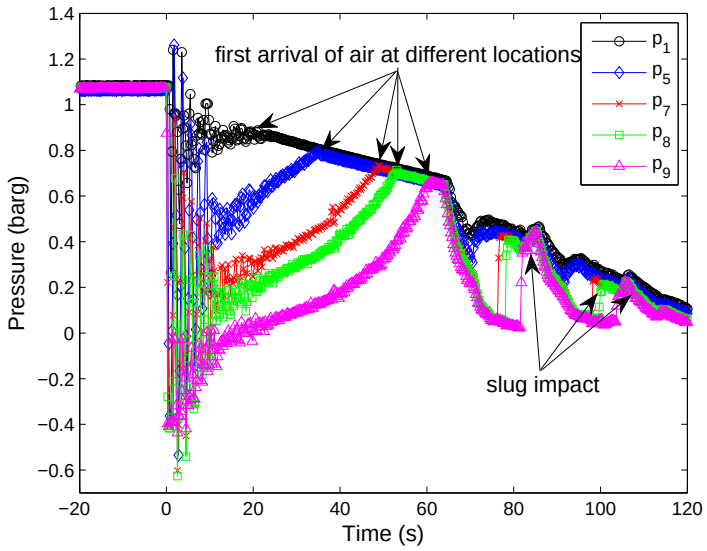

Figure 49: Pressure history at five different locations along the PVC pipeline in the emptying experiments for the intermediate case (case 10).

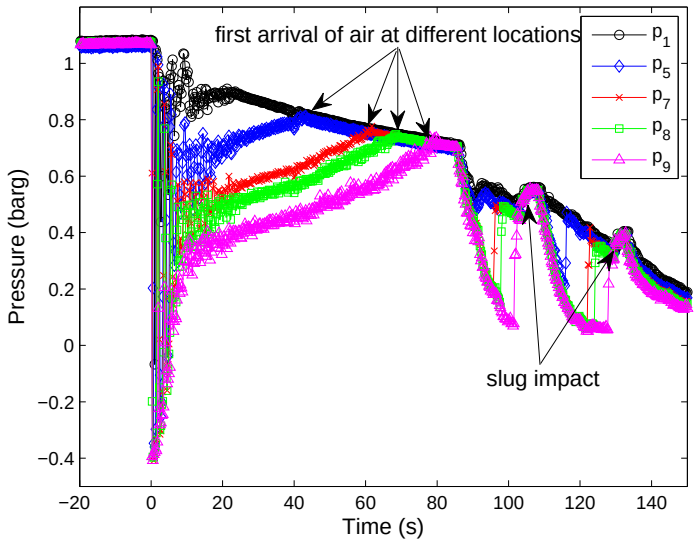

Figure 50: Pressure history at five different locations along the PVC pipeline in the emptying experiments for the gentle case (case 12).

dealing with potential fast transients, but it is difficult to solve because of the moving boundary. An attempt was the fully implicit box or Preismann finite-difference scheme in [15]. Since a fixed spatial grid and a flexible temporal grid are used in this scheme, the Courant number is time dependent. An uncontrollable large Courant number may cause a serious convergence problem. To solve this problem, the method of characteristics (MOC) was applied [16]. Since both the spatial and temporal grid are fixed in the MOC, the Courant number is constant and an interpolation has to be used to deal with the increasing water-column length. Recently, the Lagrangian particle SPH method was applied to solve the elastic model [9]. It is particularly suitable for problems with moving boundaries. In the case of large-scale pipeline emptying with compressed air supplied from the upstream end, the influence of the driving air

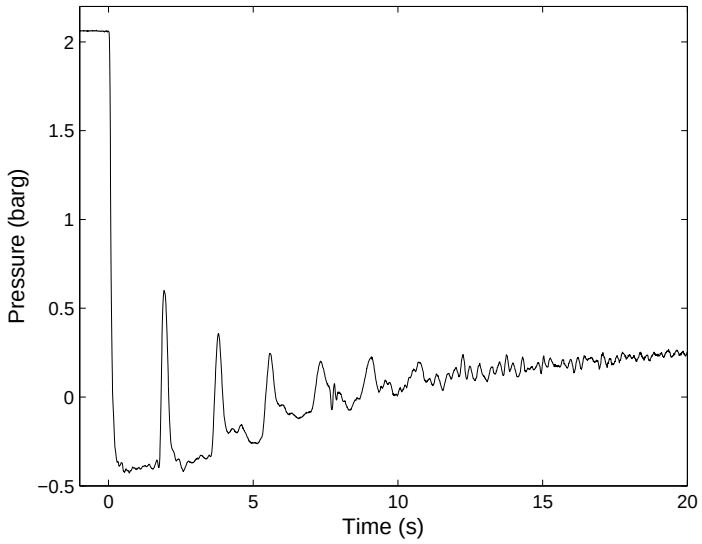

Figure 51: Pressure history at section 9 (x = 252.8 m) in case 6.

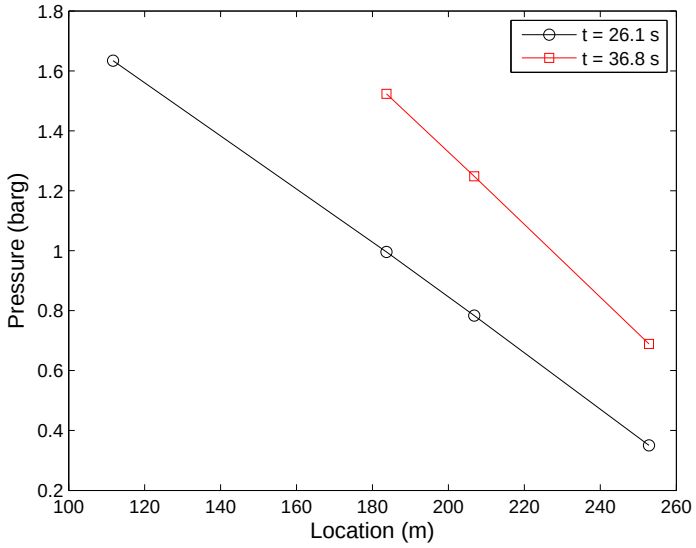

Figure 52: Pressure distribution along the water column in the emptying process (case 6) at two time levels: t = 26.1 s when the air front arrives at section 5 (x = 111.7 m) – circles and t = 36.8 s when it arrives at section 7 (x = 183.7 m) – squares. The x-coordinates of the symbols are the locations of the pressure transducers.

pressure and downstream valve resistance on the outflow rates were studied in [12]. To explore how simple models can be used to explain the phenomena observed, a control volume approach considering mass loss was proposed by Laanearu *et al.* [12]. The biggest disadvantage was that the coefficients in the model had to be calibrated from the specific experimental results by means of curve fitting.

Only the numerical results for the pipe filling process is presented herein. One is referred to our recent paper [12] for the large-scale pipe emptying problem. The rigid-column model developed in [13] with the decoupling technique [1] is applied to the current large-scale experiments. The fourth-order Runge-Kutta method is used for time marching.

The location of the pressure transducer p_u ($x = -14$ m) is taken as the upstream boundary and the measured pressure (see Fig. 17) is applied as the driving pressure. The initial water column length is $L_0 = 7.5$ m. The constant friction factor is $f = 0.0136$ (see Table 4)

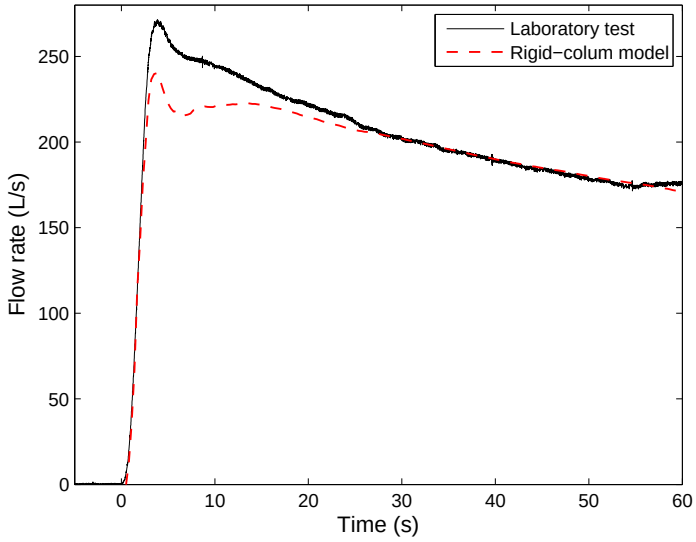

Figure 53: Flow rate history for laboratory test (solid line) and numerical simulation (dashed line).

The rigid-column solution is compared with the laboratory test in Fig. 53. The predicted flow rate history has the same trend as the experiment. The captured short-lived peak at $t = 4$ s is because of the initial peak in the driving pressure p_u. The peak deviation in the early stage is attributed to the 3D effect of the pipe bridge (complex overflow). It was found that the numerical peak flow rate is rather sensitive to the length of the upstream branch of the bridge. In addition, as mentioned in Section 2.5, the response time of the pressure transducer is approximately 1 second earlier than the flow meter. This gives some flexibility in choosing the starting time of the driving pressure. As a result, uncertainties concerning the measured pipe bridge geometry and the response time of the pressure transducer may have some effect on the peak deviation too.

The reasonable agreement between the rigid-column solution and the experimental results implies that air intrusion occurred at the advancing water front from its top has insignificant effect on the overall filling process. An important reason is that the friction mechanism in the partially stratified flow is equivalent to that in the assumed rigid column closing the pipe cross section. The fact that the intruded air is under pressure resulting in a linear pressure distribution along the water column may have some effect too.

6. Conclusions

A 275 m long pipeline of 235.4 mm diameter was filled with water and drained with compressed air within one minute time. The filling and draining processes were repeated more than 70 times and fully recorded by flow meter, pressure transducer, water level meter, void fraction meter, etc. The experiments resulted in a detailed data set for the investigation of unsteady pipe flows and air/water interface propagation and deformation.

From the examination of the pipe filling measurements it can be concluded that:

- The filling process was characterized by two stages. After the sudden opening of the upstream valve and under driving reservoir pressure, the flow quickly accelerated and reached its maximum discharge. Then followed a period of slowly decreasing discharge due to increasing pipe skin friction and increasing mass until a steady state developed.

- The original water front (water-air interface) splitted into two fronts, the velocities of which followed the inflow velocity. The stratified flow between the two water fronts had a nearly constant thickness before the occurrence of a phenomenon like hydraulic jump in open channel flow.
- Water hammer due to the rapid opening of the upstream valve did not affect the global filling process because the initial water column was short. The pressure at a location increased smoothly as a concave curve until a steady state was reached. The pressure distribution along the lengthening water column was linear, and its slope decreased with time due to the increasing length and mass. This implies that although a flow regime transition occurred, the water flow during filling behaved like a rigid column.
- The pressure of the air on top of the stratified flow was under pressure higher than atmospheric. This implies that the pressure transducer measurement cannot accurately represent the water level of the stratified flow.

From the examination of the pipe draining measurements it can be concluded that:

- The emptying process was characterized by three stages. After the sudden opening of the downstream valve, the pressurized water accelerated water-hammer wise from rest. Then followed a period of slowly increasing discharge due to decreasing driving air pressure and increasing valve resistance. Later a second rather rapid flow acceleration occurred due to reduced water mass until the air-water front visibly and audibly flushed out from the outlet.
- The initial water tail (air-water interface) gradually stratified and resulted in a water holdup and a leading air front, the velocity of which followed the outflow velocity. The stratified flow gradually decreased in height until the air reached the downstream end. Then water slugs were formed and serious slug impact took place at the downstream bend.
- Water hammer due to the rapid opening of the downstream valve affected the emptying process only in the first stage of rapid acceleration. Then the pressure at a location increased smoothly as a convex curve until the driving air was present at that point. In the stage of smoothly increasing pressure, the pressure distribution along the shortening water column was linear, and its slope increased with time due to the decreasing length and mass. This implies that although a flow regime transition occurred, the water flow during emptying after water hammer behaved like a rigid column leaking at its tail.
- The emptying process, its duration and maximum flow rate, was affected by both the driving air pressure and the downstream valve resistance. For all the valid cases, they have insignificant effect on the volume of the expelled water when the air reached at the downstream end.

Acknowledgments

The authors would like to express their sincere gratitude to staff at Deltares, Delft: Dr. Arno Kruisbrink, Dr. Christof Lubbers and Dr. Hugo Hartmann for their help in the preparation of the project HYIII-Delft-4; Richard Tuin, Martin Boele and Theo Ammerlaan for their expert technical advices during the measurement periods. The first author is grateful to the China Scholarship Council (CSC) for financially supporting his PhD studies.

References

[1] Axworthy, H. and Karney, B. W. (1997). Discussion on "Filling of pipelines with undulating elevation profiles" by Liou, C. P. and Hunt, W. A., J. Hydraul. Eng., 122(10), 534–539.

[2] Benjamin, T. B. (1968). Gravity currents and related phenomena. J. Fluid Mech., 31(2), 209–248.

[3] Bergant, A. Simpson, A. R., and Tijsseling, A. S. (2006). Water hammer with column separation: A historical review. J. Fluid. Struct., 22, 135–171.

[4] Bergant, A., van 't Westende, J. M. C., Koppel, T., Gale, J., Hou, Q., Pandula, Z. and Tijsseling, A. S. (2010). Water hammer and column separation due to accidental simultaneous closure of control valves in a large scale two-phase flow experimental test rig. Proceedings of the ASME 2010 Pressure Vessels & Piping Division / K-PVP Confrence, Bellevue, Washington, USA, CD-ROM, Paper PVP2010-26131.

[5] Bergant, A., Hou, Q., Keramat, A., and Tijsseling, A. S. (2011). Experimental and numerical analysis of water hammer in a large-scale PVC pipeline apparatus. IAHR 4-th International Meeting on Cavitation and Dynamic Problems in Hydraulic Machinery and Systems, October 26–28, 2011, Belgrade, Serbia.

[6] Cabrera, E., Izquierdo, J., Abreu, J. and Iglesias, P. L. (1996). Discussion on "Filling of pipelines with undulating elevation profiles" by Liou, C. P. and Hunt W. A., J. Hydraul. Eng., 122(10), 534–539.
[7] Crane Company (1979). Flow of Fluids through Valves, Fittings, and Pipe. Tech. Pap. 410.
[8] Guo, Q. and Song, C. S. S. (1990). Surging in urban storm drainage systems. J. Hydraul. Eng., 116(12), 1523–1537.
[9] Hou, Q., Zhang, L. X., Tijsseling, A. S. and Kruisbrink, A. C. H. (2012). Rapid filling of pipelines with the SPH particle method. Procedia Engineering, 31, 38–43.
[10] Keramat, A., Tijsseling, A. S., Hou, Q. and Ahmadi, A. (2012). Fluid-structure interaction with pipe-wall viscoelasticity during water hammer. J. Fluid. Struct., 28, 434–455.
[11] Laanearu, J., Bergant, A., Annus, I., Koppel, T. and van 't Westende, J. M. C. (2009). Some aspects of fluid elasticity related to filling and emptying of large-scale pipeline. IAHR 3-rd International Meeting on Cavitation and Dynamic Problems in Hydraulic Machinery and Systems, Brno, Czech Republic, 2009, 465–474.
[12] Laanearu, J., Annus, I., Koppel, T., Bergant, A., Vučkovič, S., Hou, Q., Tijsseling, A. S., Anderson, A. and van 't Westende, J. M. C. (2012). Emptying of large-scale pipeline by pressurized air. J. Hydraul. Eng., Accepted.
[13] Liou, C. P. and Hunt, W. A. (1996). Filling of pipelines with undulating elevation profiles. J. Hydraul. Eng., 122(10), 534–539.
[14] Lubbers, C.L. (2007). On gas pockets in wastewater pressure mains and their effect on hydraulic performance. Phd thesis, Delft University of Technology.
[15] Malekpour, A. and Karney, B. W. (2008). Rapidly filling analysis of pipelines using an elastic model. 10^{th} International Conference on Pressure Surges, Edinburgh, UK, 2008, 539–552.
[16] Malekpour, A. and Karney, B. W. (2011). Rapid filling analysis of pipelines with undulating profiles by the Method of Characteristics. ISRN Applied Mathematics, Article ID 930460.
[17] De Martino, G., Fontana, N. and Giugni, M. (2008). Transient flow caused by air expulsion through an orifice. J. Hydraul. Eng., 134(9), 1395–1399.
[18] Nydal, O. J. and Andreussi, P. (1991). Gas entrainment in a long liquid slug advancing in a near horizontal pipe. Int. J. Multiphase Flow, 17(2), 179–189.
[19] Razak, T. and Karney, B. W. (2008). Filling of branched pipelines with undulating elevation profiles. 10^{th} International Conference on Pressure Surges, Edinburgh, UK, 2008, 473–487.
[20] Shosho, C. E. and Ryan, M. E. (2001). An experimental study of the motion of long bubbles in inclined tubes. Chem. Eng. Sci., 56, 2191–2204.
[21] Tijsseling, A. S. (1996). Fluid-structure interaction in liquid-filled pipe systems: A review. J. Fluid. Struct., 10, 109–146.
[22] Vasconcelos, J. G. and Wright, S. J. (2004a). Air intrusion on pipe-filling bores in quasi-horizontal pipelines. Report UMCEE-04-01, University of Michigan, Ann Arbor, USA.
[23] Vasconcelos, J. G. and Wright, S. J. (2004b). Applications and limitations of single phase models to the description of the rapid filling pipe problem. Effective Modeling of Urban Water Systems, Monograph 13. W. James, K. N. Irvine, E. A. McBean and R. E. Pitt, Eds., CHI Publications, Ontario, Canada.
[24] Vasconcelos, J. G., Wright, S. J. and Guizani, M. (2005). Experimental investigations on rapid filling of empty pipelines. Report UMCEE-05-01, University of Michigan, Ann Arbor, USA.
[25] Wiggert, D. C. and Tijsseling, A. S. (2001). Fluid transients and fluid-structure interaction in flexible liquid-filled piping. Appl. Mech. Rev., 54, 455–481.
[26] Wylie, E. B., Streeter, V. L. and Suo, L. S. (1993). Fluid Transients in Systems. Prentice-Hall, Englewood Cliffs.
[27] Zhou, F., Hicks, F. E. and Steffler, P. M. (2002a). Observations of air-water interaction in a rapidly filling horizontal pipe. J. Hydraul. Eng., 128(6), 635–639.
[28] Zhou, F., Hicks, F. E. and Steffler, P. M. (2002b). Transient flow in a rapidly filling horizontal pipe containing trapped air. J. Hydraul. Eng., 128(6), 625–634.
[29] Zukoski, E. E. (1966). Influence of viscosity, surface tension, and inclination angle on motion of long bubbles in closed tubes. J. Fluid Mech., 25(4), 821–837.

PREVIOUS PUBLICATIONS IN THIS SERIES:

Number	Author(s)	Title	Month
12-11	J. Bogers K. Kumar P.H.L. Notten J.F.M. Oudenhoven I.S. Pop	A multiscale domain decomposition approach for chemical vapor deposition	May '12
12-12	K. Kumar T.L. van Noorden I.S. Pop	Upscaling of reactive flows in domains with moving oscillating boundaries	May '12
12-13	Q. Hou Y. Fan	Modified smoothed particle method and its application to transient heat conduction	May '12
12-14	Q. Hou A.C.H. Kruisbrink A.S. Tijsseling A. Keramat	Simulating water hammer with corrective smoothed particle method	May '12
12-15	Q. Hou A.S. Tijsseling J. Laanearu I. Annus T. Koppel A. Bergant S. Vučkovič J. Gale A. Anderson J.M.C. van 't Westende Z. Pandula A. Ruprecht	Experimental study of filling and emptying of a large-scale pipeline	May '12

Ontwerp: de Tantes,
Tobias Baanders, CWI